Combustion characteristics and pollutant emissions in transient oxy-combustion of a single biomass particle-A numerical study

Linwei Wang*, Nader Karimi, Tata Sutardi, Manosh C. Paul

*Linwei.Wang@glasgow.ac.uk

Systems, Power & Energy Research Division, School of Engineering, University of Glasgow, Glasgow G12 8QQ, United Kingdom

ABSTRACT. Oxy-combustion of biomass is a potentially attractive, and yet largely unexplored, technology facilitating the negative generation of CO_2. In this paper, numerical simulations are conducted to investigate the transient combustion process of a single biomass particle in O_2/N_2 and O_2/CO_2 atmospheres and the results are validated against the existing experimental data. Oxygen concentration varies from 27% to 100% in the investigated gaseous atmospheres. The spatiotemporal evolutions of the gas-phase temperature and species concentration fields are explored to further understand the transient combustion characteristics of biomass particles in oxygenated atmospheres. The results show considerably different burning behaviours under carbon dioxide and nitrogen containing atmospheres. Simultaneous and sequential combustion of the volatiles and char are distinguished from the numerical simulations. Further, NO_x and SO_x emissions are predicted on the basis of the validated numerical combustion model. A qualitative analysis is then performed to investigate the influences of oxygen concentration and carbon

dioxide atmosphere upon the pollutant emissions. It is shown that CO_2 has a significant inhibitory effect on NO_x formation, while it promotes SO_2 emissions. As oxygen concentration increases, the NO and SO_2 emission rates decrease under both types of gas atmospheres. Nonetheless, the overall NO_x and SO_x emissions feature different trends.

KEYWORDS. Biomass combustion; Single particle combustion; Oxy-fuel combustion; NO_x and SO_x emissions.

Nomenclature

A	pre-exponential factor	R_i	net rate of production of species i due to chemical reactions
A_p	particle surface area	s_b	Stefan-Boltzman constant, $5.67032 \times 10^{-8} \ W/m^2 \cdot K^4$
C_s	pollutant concentration	T	temperature
c_p	specific heat capacity	t	time
D_{corr}	dilution correction	u	velocity
D_i	diffusion coefficient of species i	$\vec{u}$	velocity vector
d	reaction order of related gaseous reactants	Y	mass fraction
e	reaction order of oxygen	$C_{O_2 feed}$	oxygen concentration in the injection
F_d	drag force	$C_{O_2 flue}$	oxygen concentration in the flue gas
F_{od}	oxygen-based dry factor		
f_h	fraction of heat absorbed by the particle	*Greek Symbols*	
$\vec{f_i}$	body force per unit mass	α	distribution coefficient of volatile in biomass
g_x	acceleration gravity	μ_m	molecular viscosity
$H_{reac_{cr}}$	enthalpy of reaction cr	λ	thermal conductivity
HHV	heating value of fuel	ρ	density
h_{fg}	latent heat of devolatilization	ε_p	particle emissivity

h'	enthalpy of mixture	θ_R	radiation temperature
$J_{i,j}$	molecular mass flux		
M_j	molecular weight of species j	*Subscripts*	
MP_j	weight percentage of species j	cr	char reaction number
m	mass	i	i^{th} species
Nu	Nusselt number	j	indices: 1,2,…,N
p	pressure	g	gas
Q_r	internal production rate for thermal energy	p	particle
q_j	energy flux	x, r	coordinates

1. INTRODUCTION

The growing concerns about global warming and issues around energy security have turned

renewable sources of energy into the main means of addressing world energy demands[1]. Biomass

is regarded as a promising renewable fuel and has seen an increased tendency in use. Pulverised

combustion for power generation, similar to that for coal, is perhaps the most common technology

for utilising biomass energy[2], which is being promoted world-wide[3]. Large amount of carbon

dioxide (CO_2) generated from coal fired power plants is now a serious issue and thus different

methods have been developed for carbon capture and storage (CCS)[4]. Amongst these, oxy-fuel

combustion is regarded as the most promising CCS technique for power station utilisation[4]. It is,

however, noted that provision of oxygen through low-carbon processes is an important prerequisite

to this. Due to carbon neutrality of biomass, application of CCS to biomass-fired stations can lead

to negative carbon generation, which is an attractive method of decarbonising the atmosphere.

Successful implementation of oxy-combustion of biomass requires an understanding of the

underlying physicochemical processes under O_2/CO_2 by O_2/N_2 atmospheres. Yet, some aspects of

oxy-coal/biomass combustion including the volatiles matter evolution, homogeneous reactions and

the heterogeneous combustion of char are quite complex and far from being fully understood and thus require further research.

Bu and his co-workers[5,6] studied the combustion characteristics of a single coal particle in a fluidized bed under O_2/N_2 and O_2/CO_2 gas atmospheres with mole fraction of O_2 ranging from 0% to 40%. Their results showed that, compared with O_2/N_2 atmosphere, the particle has longer ignition delay and burnout time under O_2/CO_2 atmospheres. Zhou et al.[7] studied the ignition properties and combustion characteristics of single coal particle under varying O_2/N_2 gas conditions. The results indicated that the particle temperature increases as the co-flow temperature or gas flow rate increased. Further, enhancing oxygen concentration shortens the particle ignition delay time and reduces the ignition temperature, and the influences are more obvious under high gas flow rates. Liu et al.[8] also found that the gas temperature and coal burnout fraction decrease with the replacement of N_2 by CO_2 when they combusted several high-volatile bituminous coals. These findings were later confirmed by Li et al.[9], who found that more volatiles matter is released while the reaction rates of char combustion were lower in O_2/CO_2 than O_2/N_2 gas atmospheres. Tolvanen et al.[10] investigated the combustion behaviour of char under O_2/N_2 and O_2/CO_2 environments with oxygen concentration varying from 2% to 12%. When substituting CO_2 with N_2, the rate of mass loss of char particles and, more noticeably, the surface temperature of particles decreased. Brix and his co-workers[11] found that the particle surface temperatures of char particles are higher in O_2/N_2 than those in O_2/CO_2 environments, and it increases along with enhancing oxygen concentration. Riaza et al.[12] reported that the volatiles combustion and char combustion of a single biomass particle happens sequentially in both air and oxy-fuel conditions. Under the same oxygen concentration (21%), the burnout time of the volatiles and char are longer when changing the background gas from N_2 to CO_2, while the combustion temperatures and combustion intensity

4

are reduced. Koeser et al.[13,14] visualized the volatiles and char combustion zone for single coal particles through OH-radicals images taken by high-speed laser-induced fluorescence. They found that, the ignition of coal particles is dependent on the particle size, but the larger particles have a longer ignition delay time. Most recently, Wang et al.[15] conducted a numerical simulation on the transient combustion of biomass particles in various O_2/N_2 conditions with oxygen concentration varying from 21% - 100%. These authors thoroughly investigated the unsteady heat and mass transfer and irreversibilities in the gas phase during the single biomass and coal particle devolatilisation, combustion and post-combustion stages[15,16]. They concluded that the post combustion homogenous and heterogeneous reactions have a higher impact on the gas-phase temperature and species concentration fields in higher oxygen concentration conditions, and that the entropy generated by chemical reactions tends to dominate the source of irreversibility[15,16]. Nitrogen and sulphur oxides emissions by coal and biomass combustion are of high significance due to their serious effects on the corrosion of burner equipment, photochemical smog and acid rain[17]. Substantial research effort has been made to further understand the pollutant formation and develop methods to minimize them. Svoboda et al.[18] showed that the NO_x emissions increased with increasing temperature when sub-bituminous coals burnt at 0.25MPa and 6% O_2. Valentim et al.[19] found the same trend by conducting experiments on single coal particle combustion in fluidized bed condition. Zhou et al.[20] argued that the temperature leaves little influences on the conversion of fuel-N, volatile-N and char-N to NO_x for anthracite when burning a single coal particle. Tarelho et al.[21] experimentally investigated the effects of excess air and air staging on NO formation in fluidized bed coal combustion. Increasing the excess air resulted in an increase in NO emissions, while NO emissions decreased with increasing the scale of the air staging. Li et al.[22], Duan et al.[23] and Daood et al.[24] reported that NO emissions are much lower in oxy-fuel combustion

than in air combustion. Shao et al.[25] found that the average NO_x concentration increased along with increasing oxygen concentration, and the maximum value and peak shape of the NO_x concentration curve changed with temperature. In particular, the average NO_x concentration increased from 823K to 923K and declined from 923K to 1223K. Duan et al.[26] reported that CO_2 atmosphere suppresses NH_3 yield and enhances HCN yield, and the HCN/NH_3 ratio is elevated in CO_2 atmosphere compared with that in Ar atmosphere. In Zhao's work[27], increases in temperature resulted in higher NO_x and SO_2 emissions in algae biomass combustion.

Courtemanche and Levendis[28] examined NO_x and SO_2 emissions under different equivalence ratios and temperatures and showed that higher equivalence ratios strongly decreased NO_x emissions in air combustion while increased with increasing temperature. Further, SO_2 emissions remain nearly unchanged with fuel-lean mixtures but are higher in the nitrogen-free gas than in air combustion. Croiset[29] found that SO_2 yield slightly increased through replacing N_2 by CO_2, and SO_2 emissions were similar under 28% O_2/CO_2 and 35% O_2/CO_2 but increased when oxygen concentration increased to 42%. Duan[30] reported that for coal combustion, as O_2 concentration increases in O_2/CO_2 mixture, SO_2 yield increases first and then decreases with a maximum at 30% O_2 concentration. Moron[31] argued that CO_2 atmosphere decreases the conversion ratio of sulphur in co-firing of coal and biomass particles. In contrast to this, Permchart et al.[32] suggested that, NO_x emissions highly depend on the fuel-nitrogen content and are slightly influenced by the operating conditions. Also, Liu et al.[33] reported that SO_2 emission is not affected by the combustion media, and SO_x emissions were found to be dominated by oxygen concentration rather than CO_2 atmosphere in coal combustion[34]. Hu[35] showed that SO_x emissions were similar in N_2 and CO_2 gas atmospheres, while Ren[36] reported that there are no clear links between SO_2 emission and sulphur fractions in biomass fuel.

The preceding review of literature indicates that, so far, most investigations have been focused on coal or char combustion, and there are only few studies on a single biomass particle under oxy-fuel conditions. More importantly, the existence of inconsistent, and sometimes conflicting results on NO_x and SO_x emissions highly necessitates conduction of further investigations. Thus, the current work performs a numerical study of combustion of single biomass particle under O_2/N_2 and O_2/CO_2 environments with varying oxygen concentration. The spatio-temporal distributions of the temperature and species fields are analyzed and, NO_x and SO_x emissions are evaluated to provide a deeper insight into the underlying physicochemical phenomena.

2. METHODOLOGY

2.1 Numerical model

The current numerical study is on the basis of the experiments of Ref.[37] in which a drop-tube furnace was used to study the transient combustion of single biomass particles. The particle was injection at the top, and then were ignited and burned in active O_2/N_2 and O_2/CO_2 atmospheres with oxygen concentration varying from 27% to 100%[37]. To simulate these experiments, the computational domain shown in Fig. 1 was established. In keeping with earlier works[15,16], the configuration is assumed to be axisymmetric.

The numerical simulations are conducted by using ANSYS Fluent 15.0. A Euler-Lagrange numerical model with standard k-ε turbulence model, weighted-sum-of-grey-gases model (WSGGM) and P-1 radiation model (spherical harmonic method) was implemented[38]. Further, the SIMPLE algorithm was used for velocity-pressure coupling[39] and the effect of gravity was added to the numerical simulations. The computational model simultaneously solves the following governing equations.

The conservation of mass is given by:

$$\frac{\partial \rho}{\partial t} + \frac{\partial (\rho u_x)}{\partial x} + \frac{\partial (\rho u_r)}{\partial r} + \frac{\rho u_r}{r} = 0. \tag{1}$$

Conservation of momentum in axial and radial directions read,

$$\frac{\partial (\rho u_x)}{\partial t} + \frac{\partial (\rho u_x u_r)}{\partial x} + \frac{\partial (r \rho u_x u_r)}{\partial r} \tag{2a}$$

$$= -\frac{\partial p}{\partial x} + \frac{\partial}{\partial x}\left[\mu_m \left(2\frac{\partial u_x}{\partial x} - \frac{2}{3}(\nabla \cdot \vec{u})\right)\right] + \frac{\partial}{\partial r}\left[\mu_m \left(\frac{\partial u_x}{\partial r} + \frac{\partial u_r}{\partial x}\right)\right] + \rho g_x,$$

$$\frac{\partial (\rho u_r)}{\partial t} + \frac{\partial (\rho u_x u_r)}{\partial x} + \frac{\partial (\rho u_r u_r)}{\partial r} \tag{2b}$$

$$= -\frac{\partial p}{\partial r} + \frac{\partial}{\partial x}\left[\mu_m \left(\frac{\partial u_x}{\partial r} + \frac{\partial u_r}{\partial x}\right)\right] + \frac{\partial}{\partial r}\left[\mu_m \left(2\frac{\partial u_r}{\partial r} - \frac{2}{3}(\nabla \cdot \vec{u})\right)\right] - 2\mu_m \frac{u_r}{r^2}$$

$$+ \frac{2}{3}\frac{\mu_m}{r}(\nabla \cdot \vec{u}).$$

Balance of energy for the reactive flow is written as[40,41],

$$\frac{\partial (\rho h')}{\partial t} + \frac{\partial (\rho h' u_r)}{\partial r} + \frac{\partial (\rho h' u_x)}{\partial x} = \frac{\partial p}{\partial t} - \frac{\partial q_j}{\partial (x,r)} + Q_r, \tag{3}$$

and the conservation of species is expressed by

$$\frac{\partial (\rho Y_i)}{\partial t} + \frac{\partial (\rho Y_i u_r)}{\partial r} + \frac{\partial (\rho Y_i u_x)}{\partial x} = \frac{\partial (J_{i,j})}{\partial (x,r)} + R_i. \tag{4a}$$

$$J_{i,j} = -\rho D_i \frac{\partial Y_i}{\partial (x,r)} \tag{4b}$$

The ideal gas law for the multi-component gas is written as

$$p = \rho R_u T \sum_i^N \frac{Y_i}{M_i}. \tag{5}$$

The unsteady motion of the biomass particle and energy balance was also included in the computational model. The transient motion of the particle was modelled by considering the gravitational and aerodynamic lift forces through the following equations[39].

$$m_p \frac{du_p}{dt} = F_d(u_g - u_p) + g_x(\rho_p - \rho).$$

(6)

The balance of energy for the particle is given by the following equation, which takes into account convection and radiation heat transfer and also considers phase change of the particle[39,40].

$$m_p c_{p,p} \frac{dT_p}{dt} = \pi d_p \lambda Nu(T_g - T_p) + A_p \varepsilon_p s_b(\theta_R^4 - T_p^4) + \frac{dm_p}{dt} h_{fg} - f_h \sum_{cr'} \frac{dm_p}{dt} H_{reac_{cr}},$$

(7a)

in which the Nusselt number is given by the following equation[41],

$$Nu = 2.0 + 0.6 \cdot Re_p^{1/2} \cdot (c_p \mu_g / \lambda)^{1/3}.$$

(7b)

In Eq. (7a) the term on the left-hand side represents the temporal rate of change in the sensible enthalpy of the particle. Further, the terms on the right-hand side show the effects due to convective heat transfer, thermal radiation, devolatilization and char combustion reactions, respectively. In this equation, $\frac{dm_p}{dt}$ represents the mass changes during the devolatilisation and char combustion processes and is coupled automatically by the flow solver (ANSYS-Fluent) under Discrete Phase Model (DPM) during numerical simulations[15,16].

ICEM was applied for the computational grid generation. A grid with 29925 cells was chosen after conduction of a grid-independency study with different grid densities varying from 18950 to 52680 cells. Single kinetic rate devolatilization model[42] and multiple-surface-reactions combustion model[39,43,44] were considered for the particle (see Eqs. 6 and 7). Table 1 gives the detailed chemical reaction and kinetic parameters. The properties of biomass particle are provided in Table 2, wherein the operating conditions correspond to the experiments in Ref.[37] (shown in Table 3). The

following assumptions were made during the simulations: a) The coal and biomass particles are spherical in shape, b) The gas-phase is regarded as an ideal-gas mixture.

2.2 NO$_x$ model

The formation of thermal NO$_x$ is highly temperature dependent and known as the extended Zeldovich mechanism[48]. The fuel-nitrogen forms NO$_x$ emissions via intermediates HCN and NH$_3$[49,50]. The pathways are given in Fig. 2. The principal reactions governing the formation of thermal NO$_x$ and fuel NO$_x$ are summarised in Table 4. The reaction rates proposed by Hanson and Salimiarr[51] for thermal NO$_x$ and DeSoete[52] for fuel NO$_x$ were used in the current work (see Table 4).

2.3 SO$_x$ model

The oxidation of fuel-bound sulphur is the only source of SO$_x$ emissions. During coal and biomass combustion, some of the sulphur is released as H$_2$S, COS, SO$_2$ and CS$_2$ when devolatilisation happens, while rest of the sulphur is retained in the char to be oxidized at a later stage. SO$_2$ and SO$_3$ are the final products of oxidization. For low sulphur fuels, the sulphur is regarded to mainly release as H$_2$S[53]. An eight-step mechanism[54] together with one SO$_3$ formation reaction[55] was used to describe the reaction mechanisms for sulphur oxidation. The mechanisms and chemical kinetics are shown in Table 5.

In this study, it is assumed that the fuel nitrogen and sulphur are distributed evenly between the volatiles and the char and the objective is to assess the effects of oxygen concentration and CO$_2$ on NO$_x$ and SO$_x$ emissions. Appendix A shows that changes in the distribution of nitrogen in volatiles and char do not influence the analysis in any considerable way. Furthermore, NO$_x$ and SO$_x$ emissions are predicted by post-processing as the nitrogen and sulphur contents in a single biomass particle are quite low.

2.4 Emission rates

The pollutant emission rate is introduced to compare pollutant emissions between different combustion conditions in a neutral way. The pollutant emission rate E (ng/J) is calculated by the empirical formula provided in Ref.[29]:

$$E = C_s \cdot F_{od} \cdot D_{corr}. \tag{8}$$

in which C_s (ng/m^3) is pollutant concentration, F_{od} (m^3/J) is the oxygen-based dry factor, D_{corr} is dilution correction factor. These are calculated by[29]:

$$C_s(NO) = 1.880 \cdot 10^6 \cdot [NO\ PPM] \tag{9}$$

$$C_s(SO_2) = 2.619 \cdot 10^6 \cdot [SO_2\ PPM] \tag{10}$$

$$F_{od} = \frac{R \cdot T}{P \cdot HHV} \cdot \left[\begin{array}{c} \dfrac{MP_C}{M_C \cdot C_{O_2feed}} + \dfrac{\left[\dfrac{100}{C_{O_2feed}} - 1\right] \cdot MP_H}{400 \cdot M_H} + \dfrac{MP_S}{M_S \cdot C_{O_2feed}} \\[4mm] + \dfrac{MP_N}{200 \cdot M_N} - \dfrac{\left[\dfrac{100}{C_{O_2feed}} - 1\right] \cdot MP_O}{200 \cdot M_O} \end{array} \right] \tag{11}$$

$$D_{corr} = \left[C_{O_2feed} - C_{O_2flue}\right]/C_{O_2feed} \tag{12}$$

where, R is the ideal gas constant, P is the pressure, T is the temperature, HHV is the heating value of fuel, MP_j is the weight percentage of species j in fuel, M_j is the molecular weight of species j, and C_{O_2feed} and C_{O_2flue} are the oxygen concentration in the injection and flue gas, respectively.

3. RESULTS AND DISCUSSION

3.1 Validation of numerical model

Ignition delay time, particle life time and particle maximum temperature were used to validate the numerical model by comparing with the experimental data reported in Ref.[37]. In here, the ignition delay time is defined as the time taken from the particle releasing to the moment that it is ignited. Particle life time accounts for the duration that the particle exists in the drop-tube furnace from

releasing to the extinction. Particle maximum temperature is the highest temperature that the particle experiences during the combustion process. In the experimental studies, spectral measurement was used to monitor the whole combustion process[37]. In accordance with this methodology, in the simulations the ignition and extinction moments of the particle were deduced by the start and end points of char combustion reactions ($R2 - R5$). Further, the temperature of biomass particle was tracked under the discrete phase modelling (DPM).

Tables 6, 7 and 8 depict a comparison between the simulations and experimental results of single coal and biomass particle combustion under varying gas atmospheres. In total, 81 data points were used for comparison. The tables indicate that the measured and simulated ignition delay times and particle life times are quite close and the error of particle maximum temperature is within 2.5% for all cases. The good agreement between the two datasets confirms the validity of the numerical model.

3.2 Spatio-temporal evolution of the temperature and concentration fields

Figure 3 depicts the temperature field within the near particle region for different moments after the release of particle. Figure 3a corresponds to an atmosphere consisting of 37% O_2 and 63% CO_2 on molar basis. The left most subfigure refers to 2ms after the release of the particle, which is prior to particle ignition. However, the oxidisation of volatiles (R6), which can happen almost simultaneously with the devolatilisation process (R1), has led to the formation of hot cloud of reactive gases around the particle. It is important to note that gas temperature significantly drops as the surface of the particle is approached. This is because volatiles oxidation reactions can only occur in gas-phase and the devolatilisation process is endothermic and thus cools the gas in the immediate surroundings of the particle. As the particle combustion process progresses, the temperature difference disappears but the gas around the particle still has a higher temperature

than the domain. In the late combustion stage, the particle becomes exceedingly small due to the depletion of char combustion (R2 − R5), and both the temperature and size of the reactive region decrease. Figure 3b shows the transient combustion behaviour when the particle burns in pure oxygen, which is markedly different with that under 37% O_2 and 63% CO_2 conditions (Fig. 3a). In this figure, the temperature of the burning particle at 3ms is almost 2400K. The volatiles and char combust at the same time, thus the peak temperature appears in the middle of the reactive region, and the particle and flow temperature drop significantly towards the end of the particle life time. It should be noted that as the first figure accounts for 2ms and 3ms in case a and case b, respectively and combustion is more intense at higher oxygen concentrations, the temperature difference becomes more noticeable in case a than case b. As discussed later, the temperature evolution is heavily dependent upon the oxygen concentration and type of the atmosphere.

Spatio-temporal distributions of the major chemical species have been shown in Figs. 4-7 for gas condition of 37% O_2 & 73% CO_2 and 100% O_2. Figure 4 shows the spatio-temporal distribution of CO_2 for the two specified oxygen concentrations. Due to the homogeneous reaction (R6), a large amount of CO_2 is formed immediately after the combustion of the volatiles. Yet, the CO_2 cloud diffuses quickly into the background atmosphere, which leaves the high concentration of CO_2 to the vicinity of the particle. The results of pure oxygen concentration are reported in Fig. 5b. Due to the simultaneous combustion of volatiles and char in this case, there is no concentration gradient at the centre of the CO_2 cloud. Further, in the absence of the CO_2 background gas, the cloud of CO_2 formed during the combustion process appears clearer in this figure.

The production process of CO is shown in Figure 5. When reactions R3 and R4 start with the ignition of the particle, a small amount of CO is generated in the vicinity of the particle for both investigated gas conditions. Figure 6a shows that in the case of 27% molar fraction of oxygen, the

CO cloud keeps growing as the combustion process progresses. This is driven by the high concentration of CO_2 as the background gas. The higher concentration of CO_2 leads to more CO generation through reaction R4 during the char combustion process and inhibition of oxidation of CO by reaction R7. However, under 100% O_2, CO is quickly consumed and converted to CO_2 (R7). It is important to note that in both cases CO is completely consumed at the end of the burning process.

Water vapour is a gas phase product of the combustion of volatile matters (R6) and the oxidation of hydrogen (R8). Further, water vapour reacts with char to form hydrogen and carbon monoxide through reaction $R5$. Figures 6a and 6b report the spatio-temporal distribution of H_2O for 37% O_2 & 63% CO_2 and 100% O_2, respectively. It can be clearly seen that under 37% O_2 and 63% CO_2 environment, a large cloud of water vapour appears once the volatiles combust and it diffuses into the surrounding gases, while being advected downstream. The highest concentration of water vapour cloud appears at the first milliseconds and it becomes much slighter at the last stage of particle combustion due to the continuous diffusion. Under pure oxygen environment, water vapour through the combustion of volatile matter and hydrogen reaction with oxygen is formed after the ignition of particle. It should be noted that the downstream motion of the water vapour cloud is less noticeable at higher oxygen concentration conditions. This could be related to the buoyance effects, which hinder the downstream motion of H_2O cloud in pure oxygen environment. The shorter particle life (Table 6) at higher oxygen concentration conditions also results in different positions of biomass particle and changes in H_2O cloud.

Hydrogen is produced by the reaction of water vapour and char particle (R5) and the unsteady process of hydrogen generation is depicted in Figure 7. The similar trend is observed in Figure 7a for 37% O_2 and 63% CO_2 and Fig. 8b for 100% O_2. There is no hydrogen generation prior to

ignition in Figs. 8a and 8b after 8.7ms and 3.7ms, respectively. This is to be expected as devolatilisation does not produce any hydrogen. Hydrogen has a short accumulation period after ignition but has decreased and completely disappeared at the end of the combustion process. This is because of the oxidation of hydrogen to water vapour by reaction R8. Further, a higher transient concentration of hydrogen is found in Figure 7b. There are two factors that could lead to this increase. First, the higher gas phase temperature of the reactive region and second the higher water vapour concentration surrounding the particle, which could boost reaction R5.

The time traces of mole fraction of the major gaseous species under different atmospheres during the single biomass combustion process are shown in Figure 8. The very fast release of volatile matters within the first few milliseconds of the combustion process is observed in all figures. Figures 8a and 8b present that, under O_2/N_2 environment, the amount of volatile matters keeps increasing until the moment of ignition of particle. Ignition is marked by the onset of CO (R3) and H_2 (R5) formation, which expectedly coincides with the peak point in the volatiles formation curve in Figs. 8a and 8b. It is noted that under O_2/CO_2 conditions (Figs. 8c and 8d), the peak values of the volatile matters formation curve are much smaller than that under O_2/N_2 conditions. This is because, when CO_2 is the background gas, the volatiles is ignited and starts combusting as being released from the biomass particle to the surroundings. Thus, there is no accumulation stage for the volatile matters to achieve a high peak value like in O_2/N_2 atmosphere where the volatiles is ignited much later. The difference of volatiles combustion in different background gas conditions leads to the different appearing time of CO_2 and H_2O that are mostly generated through reaction R6. Further, the concentration of H_2O starts to decrease as it reacts with char particle to form H_2 and CO (R5). The concentration of H_2 remains negligibly small during the entire burning process due to the consumption of H_2 by reaction R8. It should be noted that, the concentration of CO

increases towards a maximum value and reduces to zero at the end of the particle life time. Further, the reduction of CO life span is accelerated by the increased oxygen concentration. In conclusion, Fig. 9 confirms that, the combustion behaviour is quite different under O_2/N_2 and O_2/CO_2 conditions. This is particularly the case when the formation and consumption of volatile matters are considered.

3.3 Overall NO and SO$_2$ PPM

The overall NO and SO$_2$ PPM under varying O_2/N_2 and O_2/CO_2 conditions in the late stage (t =100ms) of single biomass particle combustion are presented in Fig. 9. Considering NO PPM (Fig. 9a), it is clearly seen that when changing the background gas from N_2 to CO_2, the overall NO PPM is sharply reduced, and is about five orders of magnitude lower in all oxygen concentrations. This is because compared with O_2/N_2 environments, there is no formation of thermal-NO_x in O_2/CO_2 atmospheres and fuel-NO_x is the only source of NO generation under this gas atmospheres. Figure 10a also indicates that thermal-NOx accounts for most NO emissions in high temperature O_2/N_2 based single particle combustion and cannot be ignored. Further, Fig. 9a shows that, under either N_2 or CO_2 based gas conditions, the higher the oxygen concentration is, the lower NO PPM emissions will be. There is a significant decrease in NO generation under O_2/N_2 atmospheres when increasing oxygen concentration, and the NO emissions generated in pure oxygen condition is negligible compared with the other cases. Under O_2/CO_2 gas conditions, the NO PPM drops sharply when oxygen concentration increases from 27% to 37%, but it decreases slightly when oxygen concentration increased up to 77% and 100%. This is because the yield of HCN and NH$_3$ are due to less CO formation and higher combustion temperature at higher oxygen concentrations[26,56].

A comparison of SO_2 PPM generations is displayed in Fig. 9b. It should be noted that, there is more SO_2 generated in CO_2 based atmospheres than that in N_2 based cases, and the difference is about two orders of magnitude. In particular, under O_2/N_2 gas atmospheres, the amount of SO_2 formed during the combustion process decreases rather moderately with increases in oxygen concentration. The case with 27% mole fraction of oxygen generates the maximum SO_2 in all investigated cases, but the difference in SO_2 generation is small when oxygen concentration rises to 37%, 77% and 100%. However, under CO_2 based gas conditions, the oxygen concentration has a much greater impact on SO_2 PPM. This is particularly the case at lower O_2 concentrations, as SO_2 PPM drops markedly when oxygen concentration increases from 27% to 77%. Yet, there is only a small difference between SO_2 generation under 77% and 100% mole fraction of oxygen.

3.4 Emission rates of NO and SO_2

The results of NO and SO_2 emission rates under varying O_2/N_2 and O_2/CO_2 atmospheres during single biomass particle combustion are presented in Figs. 10a and 10b, respectively. These figures clearly show that, in both O_2/N_2 and O_2/CO_2 gas atmospheres, the emission rates of NO and SO_2 both decrease when oxygen concentration increases from 27% to 100%. The NO emission rate differs greatly under O_2/N_2 and O_2/CO_2 atmospheres and it is much smaller when there is no nitrogen in the flow. For the emission rate of SO_2, it is about ten times larger in O_2/CO_2 than that in O_2/N_2 atmospheres. In general, the behaviour of NO and SO_2 emission rates are consistent with the changing trends of overall emissions PPM, discussed in the last section.

3.5 Generation of N and S species during combustion process

The formation process of N species (NO, NH_3, H_2S) and S species (SO_2, H_2S, SO_3) is investigated in detail by comparing with particle mass reduction during single biomass particle transient combustion. The time traces of pollutants formation compared with single biomass particle mass

loss are presented in Fig. 11. The compared pollutants formation percentage in devolatilization and char combustion stages under varying oxygen concentration conditions are shown in Fig. 12. Figures 11a-11b show the evolution process of particle mass reduction and N and S species formation when single biomass particle burning in 37% O_2/N_2 gas condition. The biomass particle loses mass rapidly as devolatilization happens and about 85% of the initial mass is lost during this process. The char combustion accounts for the remaining 15% of total mass reduction. The two proportions are quite similar to that given by the proximate analysis of the fuel. Due to the different reaction rates of devolatilization and char combustion, the changing of particle mass loss has two different slopes in these two stages, and different amounts of N and S are released at different stages of combustion. Therefore, the formation of N and S species differs as well. It can be clearly seen from Figs. 11a and 11b that, nearly all NH_3, H_2S, SO_2 and H_2S are formed during the period of particle combustion, which includes the devolatilization and char combustion stages, and the post-combustion stages contribute little. However, the amounts of NO and SO_3 keep increasing in both particle combustion stage and post-combustion stages. In particular, about 90% of NH_3, H_2S, SO_2 and H_2S are produced in the first 4ms and the other 10% are in the subsequent 6ms. These two instants, 4ms and 10ms, correspond to the particle ignition delay and particle life time when the single biomass particle burns in 37% O_2/N_2 atmosphere, indicating that about 90% of these species are formed during the devolatilization process and the rest (10%) during char combustion process. The species reach their peak amounts in the late stage of char combustion. Further, for the species of HCN and SO_2, there is no decrease after the particle vanished completely. However, a little amount of NH_3 continues to be consumed to generate more NO in the late stages of combustion and little H_2S is transferred to SO_2 which is converted to SO_3. It should be noted that only 10% of NO and SO_3 are produced during particle combustion process, and most (about 90%)

of these pollutants are generated at the post-combustion stage. This is because N_2 of the atmosphere is transferred to NO through thermal-NO_x and thus the amount of NO rises, also SO_3 is formed when SO_2 reacts with O_2.

The formation processes occurring in 77% O_2/N_2 atmosphere are shown in Figs. 11c-11d. The overall variant trend of NO_x and SO_x species is similar to that in 37% O_2/N_2 gas condition. However, the accumulation rate of NH_3 and SO_2 are much slower than those of HCN and H_2S in 77% O_2/N_2 atmosphere, while they are quite close under 37% O_2/N_2 gas condition. Further, the consumption rate of NH_3 during the post-combustion stage is much faster in higher oxygen concentration conditions. This is because the higher oxygen concentration accelerates the conversion rates of NH_3 to NO and SO_2 to SO_3. Moreover, the inflection points, which indicate the different slopes and stages correspond to biomass particle combustion in 77% O_2/N_2 atmosphere. The first inflection point is around 5ms and the time for HCN and SO_2 reaching peak value is almost 11ms.

Figures 11e-11f present the mass and emissions species evolution process under 37% O_2/CO_2 atmosphere. Evidently, replacing N_2 by O_2 influences the formation process of the pollutants significantly. NO, HCN, SO_2 continue to increase monotonically, while they feature three different stages. The first stage corresponds to 0-4ms, which is the particle ignition delay time. At this stage, about 10% of the total NO, HCN and SO_2 are formed. The second stage is 4-18ms and is related to the char combustion process. The generation rates of NO, HCN and SO_2 become larger at this stage and eventually 50% of NO, 60% of HCN and 50% of SO_2 are produced. After the extinction of the biomass particle, the amounts of NO, HCN and SO_2 keep increasing at a slower rate and the formation process of these species continues. For NH_3 and H_2S, the species accumulate at the beginning with three different increasing rates and they decrease later. In addition, compared with

37% O_2/N_2 gas condition, less NH_3 but more H_2S are consumed in the post-combustion stages in 37% O_2/CO_2 gas condition. Considering the formation of SO_3, the partition of SO_3 formed during the particle existing stage (0-18ms) only accounts for about 2% of the total SO_3 emissions. Almost all SO_3 is generated after the particle burning out. The amount formed during 0-18ms only accounted for about 2% of the total pollutant formation. Figures 11g-11h illustrate the results of 77% O_2/CO_2 gas condition. About 25% of NO and SO_2 and 30% of HCN are produced during the particle ignition delay time (0-5ms). Another 25% NO and SO_2 and 30% HCN are formed during the char combustion process (5ms-11ms), while the rest are formed in the post-combustion process. Overall, Fig. 12 implies that the emission formation processes are quite different in O_2/CO_2 atmosphere in comparison to those in O_2/N_2 atmospheres. As there is no N_2 in the CO_2 based atmospheres, all NO is generated from the fuel-N. Therefore, the NO shares the same trend as HCN when particle combusts in O_2/CO_2 atmosphere. Meanwhile, CO_2 in the atmosphere can restrain the reaction rates of fuel-N and fuel-S, especially volatile-N and volatile-S, and then extends the conversion time of fuel-N and fuel-S are converted to NO_x and SO_x species.

Next, the percentages of HCN, NH_3, SO_2 and H_2S formed in different atmospheres during devolatilization and char combustion process (Devol- and Char- respectively) are compared to explore the influences of oxygen concentration and CO_2 atmosphere upon the pollutants formation. The results are shown in Figure 12. Under O_2/N_2 gas atmospheres, over 80% of the N-intermediate HCN is formed during the devolatilization process and less than 20% is formed during the char combustion process. Further, the oxygen concentration does not significantly affect the formation percentage. Devol- HCN slowly declines from 89.7%, 87.5%, 85.35% to 81.67% when oxygen concentration changes from 27% to 100%. Char-HCN slightly increases from 9.89%, 12.4%, 14.55% to 18.29%. Nevertheless, under O_2/CO_2 gas atmospheres, the effect of oxygen concentration on

the formation of HCN is more obvious. Higher concentrations of oxygen greatly prompt the production of Devol-HCN and thus less HCN is formed during char combustion. A similar change of trend is found for devol-NH_3 in O_2/CO_2 and Char-NH_3 under both O_2/N_2 and O_2/CO_2 gas atmospheres along with the changing of oxygen concentration. The formation percentage of Devol-NH_3 under O_2/N_2 environments nearly keeps at 89% when the oxygen concentration increases from 27% to 100%.

Considering the formation of SO_2, the Devol-SO_2 and Char-SO_2 show the opposite changing trends in O_2/N_2 and O_2/CO_2 gas atmospheres. Volatile-SO_2 decreases while char-SO_2 increased when oxygen concentration becomes larger under O_2/N_2 gas conditions. By replacing N_2 with CO_2, the changing trends of Devol-SO_2 and Char-SO_2 are opposite each other when oxygen concentration increases. Volatile-SO_2 only accounts for 5.94% of the total SO_2 in 37% O_2, but it rises to 19.74% in 77% O_2 and further up to 69.15% for 100% O_2. The proportion of Char-SO_2 accounts from 40.55%, 20.75% to 28.71% of the SO_2 emission accordingly. The similar trend is found when considering the effects of oxygen concentration on the formation of H_2S during different combustion stages. Under O_2/N_2 environments, the maximum formation percentage of H_2S during the devolatilization stage appears at the lowest oxygen concentration (27%). While under O_2/CO_2 environments, char-H_2S dominates the H_2S formation in lower oxygen concentration conditions instead.

4. CONCLUSIONS

A set of numerical simulations on combustion of single biomass particle under different O_2/N_2 and O_2/CO_2 atmospheres were conducted, and the results were compared against the outcomes of an existing experimental work. The main objective was to gain further understanding of the general behaviour of transient burning of a biomass particle in oxygenated atmospheres as the central

component of oxy-biomass-combustion technology. The spatiotemporal distributions of the gas-phase temperature and major chemical species were obtained using the validated numerical combustion model. Further, a qualitative analysis on the emission characteristics of NO_x and SO_x pollutants was conducted. The main findings of this work can be summarised as follows.

- The combustion behaviour of single biomass particle is significantly different in O_2/N_2 and O_2/CO_2 atmospheres. The volatile matters combust prior to the ignition of the particle in O_2/CO_2, while the volatiles and chars combust sequentially in O_2/N_2 conditions.

- Under CO_2 atmospheres, the production and depletion process of CO is majorly affected by the large amount of CO_2 existing in the background gas.

- It was found that more NO_x is emitted in O_2/N_2 atmospheres than in O_2/CO_2 due to the strong formation of thermal NO_x. Yet, there is less SO_2 emission in nitrogen containing atmosphere compared to those in carbon dioxide containing atmospheres.

- NO emission rate is higher in O_2/N_2 than O_2/CO_2 atmospheres, while SO_2 emission rate has the opposite trend. When oxygen concentration increases, the emission rates of NO and SO_2 decreased under both atmospheres.

- In O_2/CO_2 atmospheres, oxygen concentration has a greater influence on the formation of NO_x. Finally, SO_x pollutants are observed to be quite sensitive to oxygen concentration in both O_2/N_2 and O_2/CO_2 environments.

ACKNOWLEDGEMENTS

REFERENCES

1. Furnel, S.; Marcos, B.; Godbout, S.; etc. Predicting gaseous emissions from small-scale combustion of agricultural biomass fuels. *Bioresource Technology* **2015**, 179, 165-172.

2. Energy outlook 2012. International Energy Agency, 2012.

3. Stanislav, V.V.; David, B.; Lars, K.A. An overview of the chemical composition of biomass. *Fuel* **2010**, 89, 913-933.

4. Buhre, B.J.P.; Elliott, L.K.; Sheng, C.D.; etc. Oxy-fuel combustion technology for coal-fired power generation. *Progress in Energy and Combustion Science* **2005**, 31, 283–307.

5. Bu, C.S.; Liu, D.Y.; Chen, X.P.; etc. Ignition behavior of single coal particle in a fluidized bed under O_2/CO_2 and O_2/N_2 atmospheres: A combination of visual image and particle temperature. *Applied Energy* **2014**, 115, 301-308.

6. Bu, C.S.; Pallares, D.; Chen, X.P.; etc. Oxy-fuel combustion of a single fuel particle in a fluidized bed: char combustion characteristics, an experimental study. *Chemical Engineering Journal* **2016**, 287, 649-656.

7. Zhou, K., Lin, Q.Z., Hu, H.W.; etc. The ignition characteristics and combustion processes of the single coal slime particle under different hot-coflow conditions in N_2/O_2 atmosphere. *Energy* **2017**, 136, 173-184.

8. Liu, H.; Zailani, R.; Gibbs, B.M. Comparisons of pulverized coal combustion in air and in mixtures of O_2/CO_2. *Fuel* **2005**, 84, 833-840.

9. Li, X.C.; Rathnam, R.K.; Yu, J.L.; etc. Pyrolysis and combustion characteristics of an Indonesian low-rank coal under O_2/N_2 and O_2/CO_2 conditions. *Energy & Fuels* **2010**, 24(1), 160-164.

10. Tolvanen, H.; Raiko, R. An experimental study and numerical modeling of combustion two coal chars in a drop-tube reactor: A comparison between N_2/O_2, CO_2/O_2 and $N_2/CO_2/O_2$ atmospheres. *Fuel* **2014**, 124, 190-201.

11. Brix, J.; Navascues, L.G.; Nielsen, J.B.; etc. Oxy-fuel combustion of millimeter-sized coal char: Particle temperatures and NO formation. *Fuel* **2013**, 106, 72-78.

12. Riaza, J.; Khatami, R.; Levendis, Y.A.; etc. Combustion of single biomass particles in air and in oxy-fuel conditions. *Biomass & Bioenergy* **2014**, 64, 162-174.

13. Koser, J.; Becker, L.G.; Vorobiev, N.; etc. Characterization of single coal particle combustion within oxygen-enriched environments using high-speed OH-PLIF. *Applied Physics B: Lasers and Optics* **2015**, 121, 459-464.

14. Koser, J.; Becker, L.G.; GoBmann, A.; etc. Investigation of ignition and volatile combustion of single coal particles within oxygen-enriched atmospheres using high-speed OH-PLIF. *Proceedings of the Combustion Institute* **2017**, 36, 2103-2111.

15. Wang, L.W.; Karimi, N.; Sutardi, T.; etc. Gas-phase transport and entropy generation during transient combustion of single biomass particle in varying oxygen and nitrogen atmospheres. *International Journal of Hydrogen Energy* **2018**, 43(17), 8506-8523.

16. Wang, L.W.; Karimi, N.; Paul, M.C. Numerical modelling of unsteady transport and entropy generation in oxy-combustion of single coal particles with varying flow velocities and oxygen concentrations. *Applied Thermal Engineering* **2018**, 144, 147-164.

17. Dong, L.; Gao, S.; Song, W.; etc. NO reduction in decoupling combustion of biomass and biomass-coal blend. *Energy & Fuels* **2008**, 23(1), 224-228.

18. Svoboda, K.; Pohorely, M. Influence of operating conditions and coal properties on NOx and N_2O emissions in pressurized fluidized bed combustion of subbituminous coals. *Fuel* **2014**, 83, 1095-1103.

19. Valentim, B.; Lemos de Sousa, M.J.; Abella, P.; etc. Combustion studies in a fluidised bed— The link between temperature, NOx and N_2O formation, char morphology and coal type. *International Journal of Coal Geology* **2006**, 67, 191-201.

20. Zhou, H.; Huang, Y.; Mo, G.Y.; etc. Experimental investigations of the conversion of fuel-N, volatile-N and char-N to NOx and N_2O during single coal particle fluidized bed combustion. *Journal of Energy Institute* **2017**, 90(1), 62-72.

21. Tarelho, L.A.C.; Matos, M.A.A.; Pereira, F.J.M.A. Influence of limestone addition on the behaviour of NO and N_2O during fluidised bed coal combustion. *Fuel* **2006**, 85, 967-977.

22. Li, W.; Li, S.Y.; Ren, Q.Q.; etc. Study of oxy-fuel cola combustion in a 0.1MWth circulating fluidized bed at high oxygen concentrations. *Energy & Fuels* 2014, 28, 1249-1254.

23. Duan, L.B.; Duan, Y.Q.; Zhao, C.S.; etc. NO emission during co-firing coal and biomass in an oxy-fuel circulating fluidized bed combustor. *Fuel* **2015**, 150, 8-13.

24. Daood, S.S.; Javed, M.T.; Gibbs, B.M.; etc. NO_x control in coal combustion by combining biomass co-firing, oxygen enrichment and SNCR. *Fuel* **2013**, 105, 283-292.

25. Shao, L.M.; Fan, S.S.; Zhang, H.; etc. SO_2 and NO_x emissions from sludge combustion in a CO_2/O_2 atmohphere. *Fuel* **2013**, 109, 178-183.

26. Duan, L.B.; Zhao, C.S.; Ren, Q.Q.; etc. NO_x precursors evolution during coal heating process in CO_2 atmosphere. *Fuel* **2011**, 90, 1668-1673.

27. Zhao, B.T.; Su, Y.X.; Liu, D.Y.; etc. SO_2/NO_x emissions and ash formation from algae biomass combustion: Process characteristics and mechanisms. *Energy* **2016**, 113, 821-830.

28. Courtemanche, B.; Levendis, Y.A. A laboratory study on the NO, NO_2, SO_2, CO and CO_2 emissions from the combustion of pulverized coal, municipal waste plastics and tires. *Fuel* **1998**, 77(3), 183-196.

29. Croiset, E.; Thambimuthu, K.V. NO_x and SO_2 emissions from O_2/CO_2 recycle coal combustion. *Fuel* 2001, 80, 2117-2121.

30. Duan, L.B.; Zhao, C.S.; Zhou, W.; etc. Sulfur evolution from coal combustion in O_2/CO_2 mixture. *Journal of Analytical and Applied Pyrolysis* 2009, 86, 269-273.

31. Moron, W.; Rybak, W. NO_x and SO_2 emissions of coals, biomass and their blends under different oxy-fuel atmospheres. *Atmospheric Environment* **2015**, 116, 65-71.

32. Permchart, W.; Kouprianov, V.I. Emission performance and combustion efficiency of a conical fluidized-bed combustor firing various biomass fuels. *Bioresource Technology* **2004**, 92, 83-91.

33. Liu, H.; Chaney, J.; Li, J.X.; etc. Control of NO_x emissions of a domestic/small-scale biomass pellet boiler by air staging. *Fuel* **2013**, 103, 792-798.

34. Zheng, L.G.; Furimsky, E. Assessment of coal combustion in O_2+CO_2 by equilibrium calculations. *Fuel Processing Technology* **2003**, 81, 23-34.

35. Hu, Y.; Naito, S.; Kobayashi, N.; etc. CO_2, NO_x and SO_2 emissions from the combustion of coal with high oxygen concentration gases. *Fuel* **2000**, 79, 1925-1932.

36. Ren, X.H.; Sun, R.; Meng, X.X.; etc. Carbon, sulphur and nitrogen oxide emissions from combustion of pulverized and torrefied biomass. *Fuel* **2017**, 188, 310-323.

37. Khatami, R.; Stiver, C.; Joshi, K.; etc. Combustion behaviour of single particles from three different coal ranks and from sugar cane bagasse in O_2/N_2 and O_2/CO_2 atmospheres. *Combustion and Flame* **2012**, 159, 1253-1271.

38. Hurt, R.H. Structure, properties and reactivity of solids fuels. *In: 27th Symposium (International) on Combustion, The Combustion Institute* **1998**, 2887-2904.

39. ANSYS Fluent Theory Guide 15.0. 2013.

40. Blaid S. Ph.D. thesis. Numerical investigation of the combustion processes of various fuels. University of Glasgow, 2015.

41. Ranz, W.E.; Marshall, W.R. Evaporation from Drops, Part I and Part II. *Chemical Engineering Progress* **1952**, 48(4), 173-180.

42. Badzioch, S.; Hawksley, P.G.W. Kinetics of thermal decomposition of pulverized coal particles. *Industrial & Engineering Chemistry Process Design and Development* **1970**, 9(4), 521-530.

43. Chen, X.; Horio, M.; Kojima, T. Numerical simulation of entrained flow coal gasifiers. Part I: modeling of coal gasification in an entrained flow gasifier. *Chemical Energy Science* **2000**, 55, 3861-3874.

44. Mayers, A.M. The rate of reduction of carbon dioxide by graphite. *Journal of the American Chemical Society* **1934**, 56, 70-76.

45. Howard, J.B.; Williams, G.C.; Fine, D.H. Kinetics of carbon monoxide oxidation in postflame gases. *Proceedings of 14th Symposium (International) on Combustion* **1973**, 975-986.

46. Serio, M.A.; Hamblen, D.G.; Markham, J.R.; etc. Kinetics of volatile product evolution in coal pyrolysis: experiment and theory. *Energy & Fuels* **1987**, 1, 138-152.

47. Spliethoff, H. Power generation from solid fuels. Springer Heidelberg Dordrecht, London, New York, 2010.

48. Zeldovich, Y.B. The oxidation of nitrogen in combustion and explosions. *Acta Physicochem USSR* **1964**, 21, 577-628.

49. Miller JA, Fisk GA. Chemical and Engineering News. 1987, 31.

50. Houser, T.J.; Hull, M.; Always, R.; etc. Kinetics of formation of hydrogen cyanide during pyridine pyrolysis. *International Journal of Chemical Kinetics* **1980**, 12(8), 569-574.

51. Hanson, R.K.; Salimian, S. Survey of rate constants in H/N/NO systems. In W.C. Gardiner, New York, 1984.

52. Desoete, G.G. Overall reaction rates of NO and N_2 formation from fuel nitrogen. *Symposium (International) on Combustion* **1975**, 15(1), 1093-1102.

53. Molero de Blas, L.J. Pollutant Formation and Interaction in the Combustion of Heavy Liquid Fuels. PhD thesis. University of London, England. 1998.

54. Kramlich, J.C. The fate and behaviour of fuel-sulfur in combustion systems. PhD thesis, 1980. Washington State University, Washington, USA.

55. Hunter, S.C. Formation of SO_3 in gas turbines. *Transactions of the ASME* **1982**, 104,44-51.

56. Glarborg, P., Jensen, A.D., Johnsson, J.E. Fuel nitrogen conversion in solid fuel fired systems. *Progress in Energy and Combustion Science* 2003, 29(2), 89-113.

Table 1. Chemical reactions and kinetic constants of biomass combustion

Reaction NO.	Reaction Mechanism	Kinetic parameters			d	e	Ref.
		A (unit vary)	E (J/kmol)	b			
R1	Biomass $\rightarrow$ α Volatile $+ (1 - \alpha)$ Char	3.12E+05	7.4E+07	-	-	-	Ref[39]
R2	$C_{(s)} + O_2 \rightarrow CO_2$	0.002	7.9E+07	0	-	-	Ref[39]
R3	$C_{(s)} + 0.5\ O_2 \rightarrow CO$	0.052	1.33E+08	0	-	-	Ref[43]
R4	$C_{(s)} + CO_2 \rightarrow 2\ CO$	4.4	1.62E+08	1	-	-	Ref[44]
R5	$C_{(s)} + H_2O \rightarrow H_2 + CO$	1.33	1.47E+08	1	-	-	Ref[44]
R6	Volatile $+ O_2 \rightarrow CO_2 + H_2O$	2.119E+11	2.027E+08	-	0.2	1.3	Ref[39]
R7	$CO + 0.5\ O_2 \rightarrow CO_2$	1.30E+11	1.26E+08	-	0.5	0.5	Ref[45]
R8	$H_2 + 0.5\ O_2 \rightarrow H_2O$	5.69E+11	1.465E+08	-	1	0.5	Ref[45]

Table 2. Fuel Properties[37]

Fuel	Biomass: Bagasse
Proximate analysis (received)	
C	4.4
Volatile (%)	83.9
Fixed Carbon (%)	7.7
Ash (%)	4.0
Ultimate analysis (dry basis)	
C	44.3
H	5.7
O	45.5
N	0.2
S	0.07
Ash	4.2
Heating value dry fuel (MJ/kg)	16.3

Table 3. Operating conditions of the experiment[37]

Parameters	Values
Wall Temperature	1400 K
Temperature of injecting gas	1200 K
Velocity of gas	4.55 cm/s
Diameter of particles	80 μm
Initial temperature of particles	1050 K
Velocity of particles	15 cm/s

Table 4. Chemical reactions and kinetic constants of NOx formation

Reaction NO.	Reaction Mechanism	A (1/s)	β	E (J/mol)	Ref
$R9$	$O + N_2 \rightleftharpoons N + NO$	1.8E+08	0	38370	Ref[48]
		3.8E+07	0	425	Ref[48]
$R10$	$N + O_2 \rightleftharpoons O + NO$	1.8E+04	1	4680	Ref[48]
		3.8E+03	1	20820	Ref[48]
$R11$	$N + OH \rightleftharpoons H + NO$	7.1E+07	0	450	Ref[48]
		1.7E+08	0	24560	Ref[48]
$R12$	$HCN + O_2 \rightarrow NO + \cdots$	1.0E+10	0	280451.95	Ref[49,50]
$R13$	$NH_3 + O_2 \rightarrow NO + \cdots$	4.0E+06	0	133947.2	Ref[49,50]
$R14$	$HCN + NO \rightarrow N_2 + \cdots$	3.0E+12	0	251151	Ref[49,50]
$R15$	$NH_3 + NO \rightarrow N_2 + \cdots$	1.8E+08	0	113017.95	Ref[49,50]

Table 5. Chemical reactions and kinetic constants of SOx formation

Reaction NO.	Reaction Mechanism	A (1/s)	β	E (J/mol)	Ref
$R16$	$H_2S + H \rightleftharpoons SH + H_2$	1.8E+07	0	7480	Ref[54]
		9.37E+06	0	62500	Ref[54]
$R17$	$OH + H_2S \rightleftharpoons H_2O + SH$	1.38E+02	0	3740	Ref[54]
		3.11E+07	0	122000	Ref[54]
$R18$	$SO + OH \rightleftharpoons H + SO_2$	1.62E+08	0	2560	Ref[54]
		7.69E+09	0	119000	Ref[54]
$R19$	$SH + O \rightleftharpoons SO + H$	3.55E+08	0	2690	Ref[54]
		2.99E+09	0	169000	Ref[54]
$R20$	$O + H_2S \rightleftharpoons SH + OH$	4.36E+03	0	13800	Ref[54]
		9.88E+08	0	6.04E+04	Ref[54]
$R21$	$SO + O_2 \rightleftharpoons SO_2 + O$	4.47E+05	0	2.70E+04	Ref[54]
		1.66E+06	0	7.61E+04	Ref[54]
$R22$	$H + SH \rightleftharpoons H_2S$	1.10E+03	0	0	Ref[54]
		8.67E+14	0	3.82E+05	Ref[54]
$R23$	$SO + O \rightleftharpoons SO_2$	8.71E+09	-1.8	4.12E+03	Ref[54]
		1.91E+14	0	5.21E+05	Ref[54]
$R24$	$SO_2 + O \rightleftharpoons SO_3$	3.63E+12	0	4.12E+03	Ref[55]
		7.41E+14	0	-3.46E+05	Ref[55]

Table 6 Summary cases and compared results of Bagasse (Active Flow)

Case	Gas Conditions	Ignition Delay Time (ms)		Particle Life Time (ms)		Particle Maximum Temperature (K)		
		Experiment[37]	Numerical Simulation	Experiment[37]	Numerical Simulation	Experiment[37]	Numerical Simulation	Error (%)
1	21% O_2 79% N_2	3	3.2	18	18.3	1900	1891.716	0.44
2	27% O_2 73% N_2	9	8.8	18	17.8	2150	2100.44	2.31
3	37% O_2 63% N_2	4	3.9	10	10.4	2370	2386.658	0.70
4	77% O_2 23% N_2	5	5.1	11	11.8	2700	2702.918	0.11
5	100% O2	3	3.2	8	8.1	2950	2926.125	0.81
6	27% O_2 73% CO_2	9	9.4	40	39.6	1630	1635.702	0.35
7	37% O_2 63% CO_2	4	4.3	19	18.0	2280	2266.177	0.61
8	77% O_2 23% CO_2	5	5.4	12	11.3	2650	2652.378	0.09

Table 7 Summary cases and compared results of DECS-11 (Active Flow)

Case	Gas Conditions	Ignition Delay Time (ms)		Particle Life Time (ms)		Particle Maximum Temperature (K)		
		Experiment[37]	Numerical Simulations	Experiment[37]	Numerical Simulations	Experiment[37]	Numerical Simulations	Error (%)
1	21% O_2 79% N_2	5	5.1	42	41.9	2000	1972.85	1.36
2	27% O_2 73% N_2	5	5.2	38	38.6	2420	2431.001	0.45
3	37% O_2 63% N_2	6	6.5	32	32.7	2400	2385.15	0.62
4	68% O_2 32% N_2	6	5.1	18	17.1	2950	2919.957	1.02
5	100% O_2	6	5.9	19	19.2	2900	2889.129	0.37
6	27% O_2 73% CO_2	5	5.4	52	50.9	1980	1981.821	0.09
7	37% O_2 63% CO_2	6	5.4	32	33.0	2300	2268.487	1.37
8	68% O_2 32% CO_2	6	5.1	18	17.1	2950	2991.13	1.39

Table 8 Summary cases and compared results of DECS-11 (Quiescent Flow)

Case	Gas Conditions	Ignition Delay Time (ms)		Particle Life Time (ms)		Particle Maximum Temperature (K)		
		Experiment[37]	Numerical Simulations	Experiment[37]	Numerical Simulations	Experiment[37]	Numerical Simulations	Error (%)
1	20% O_2 80% N_2	16	16.2	75	77.3	2300	2096.389	8.85
2	30% O_2 70% N_2	17	17.6	58	57.4	2406.5	2367.095	1.64
3	40% O_2 60% N_2	17	16.8	50	47.8	2612.5	2578.168	1.31
4	60% O_2 40% N_2	14	14.4	37	38.5	2781.5	2699.928	2.93
5	80% O_2 20% N_2	13	13.6	30	33.6	3050	3033.645	0.54
6	100% O_2	11	10.6	27	28.2	3094	3070.951	0.74
7	20% O2 80% CO_2	21	21.2	113	107.9	2125	2125.618	0.03
8	30% O_2 70% CO_2	19	19.3	70	72.1	2250	2217.894	1.43
9	40% O_2 60% CO_2	17	17.1	57	56.4	2406.5	2364.946	1.73
10	60% O_2 40% CO_2	13	12.9	40	40.6	2650	2635.344	0.55
11	80% O_2 20% CO_2	12	11.7	32	32.3	2968.8	2954.358	0.49
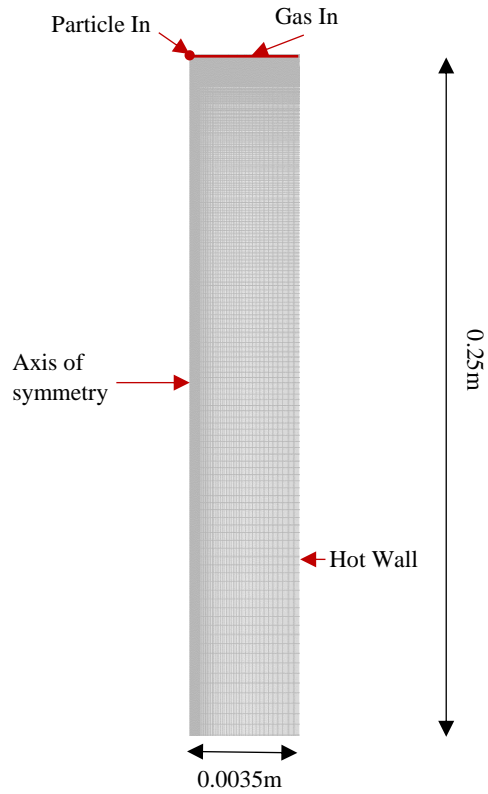
Figure 1. Schematic of Axis-symmetric domain used for the numerical simulations.
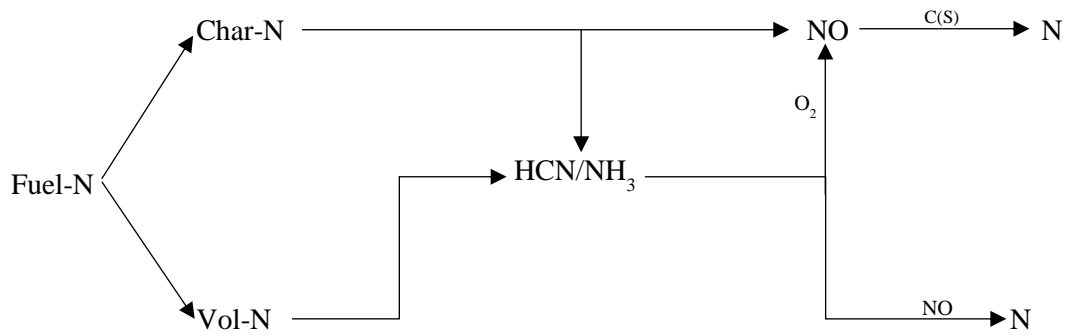
Figure 2. Fuel-NO$_x$ pathways[49,50].

(a)

Particle releasing point and dropping direction

(b)
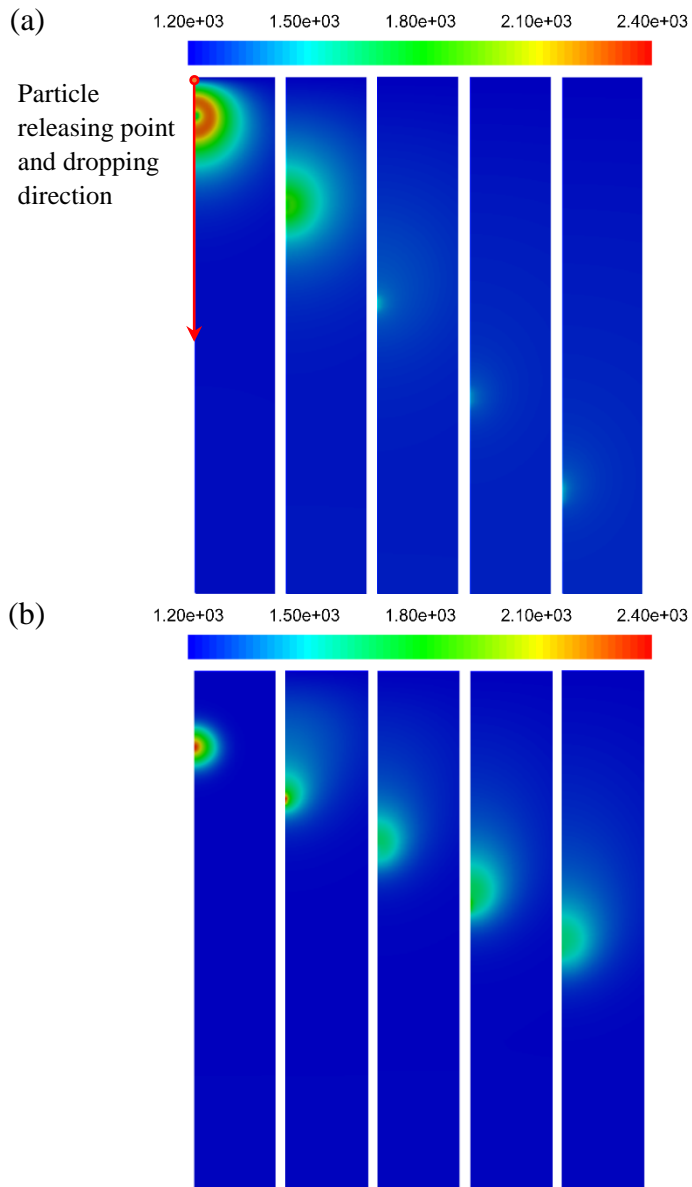
Figure 3. Spatio-temporal distribution of the gas temperature: (a) 37% O_2/CO_2 (2ms, 6ms, 10ms, 14ms, 18ms), (b) 100% O_2 (3ms, 5ms, 7ms, 9ms, 11ms).
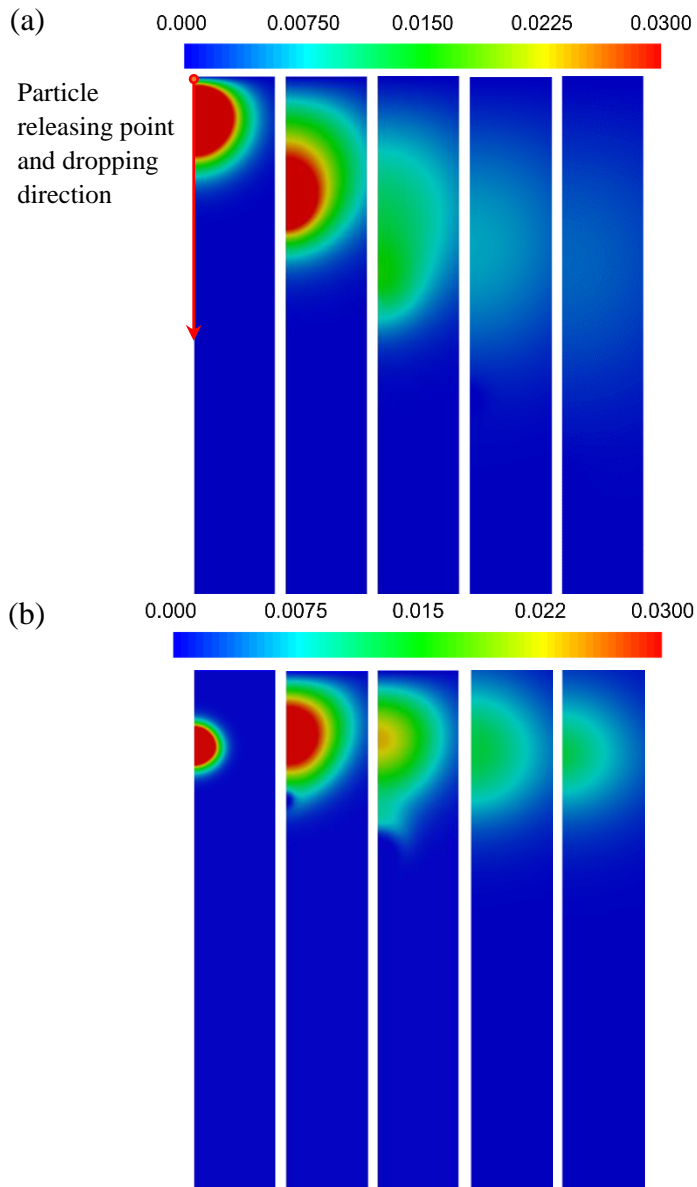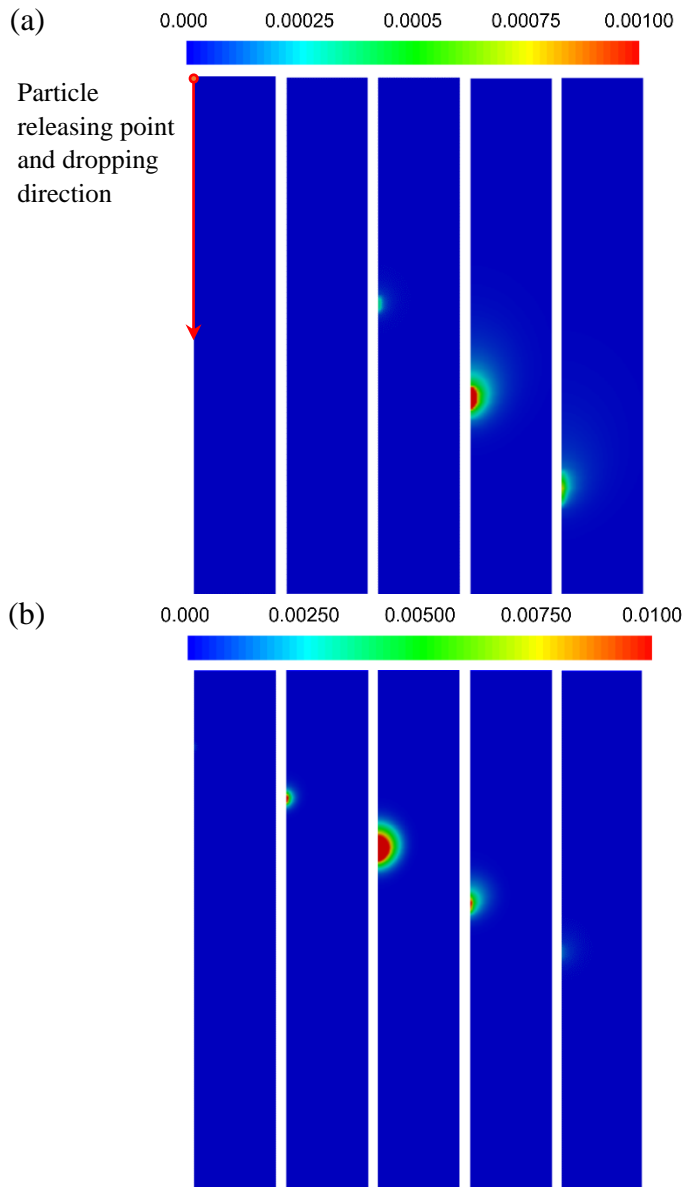
(a)

Particle releasing point and dropping direction

(b)
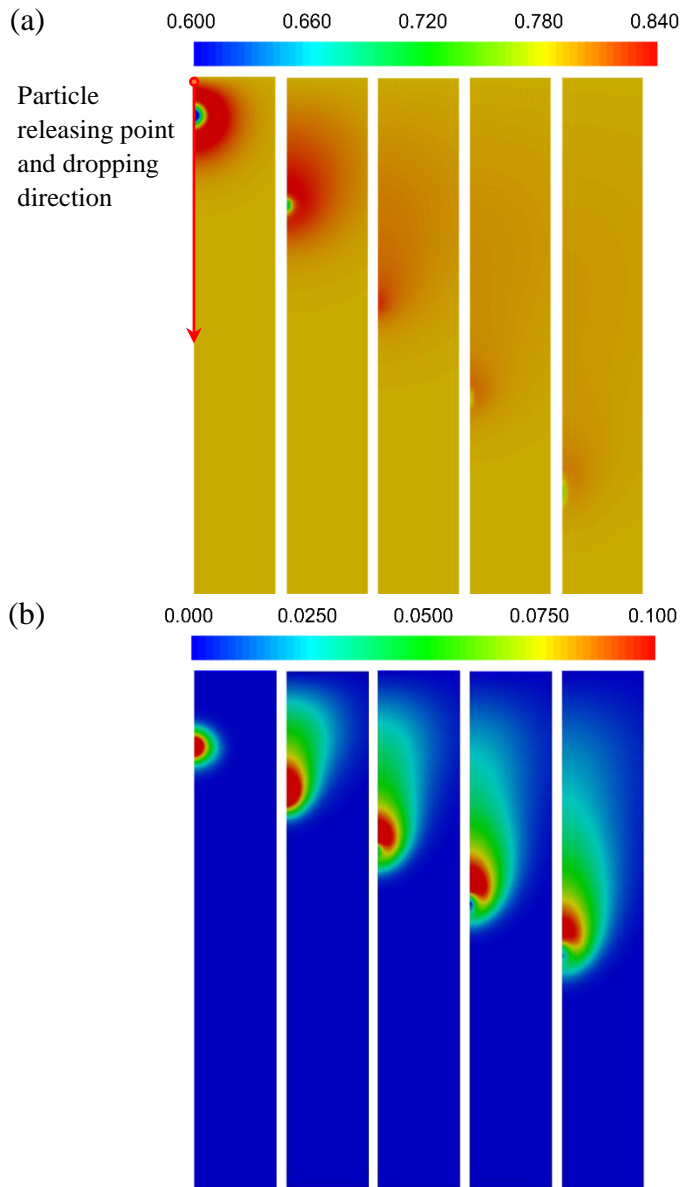
Figure 4. Spatio-temporal distribution of the mass fraction of CO_2: (a) 37% O_2/CO_2 (2ms, 6ms, 10ms, 14ms, 18ms), (b) 100% O_2 (3ms, 5ms, 7ms, 9ms, 11ms).
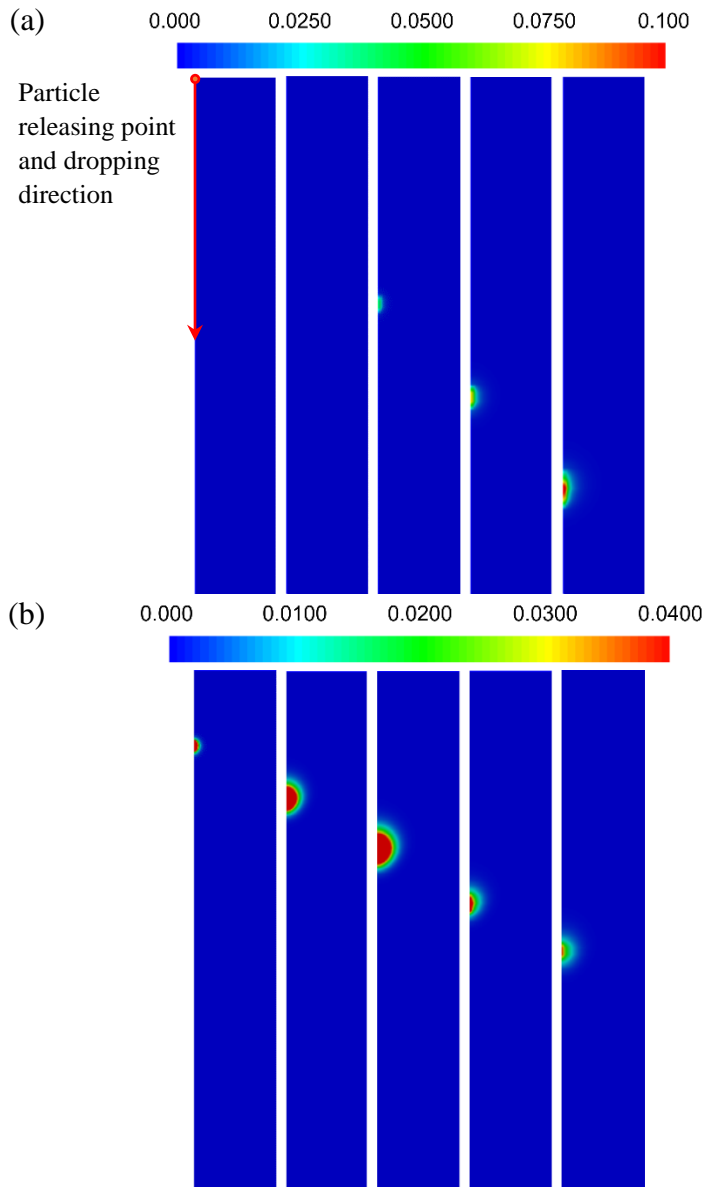
Figure 5. Spatio-temporal distribution of the mass fraction of CO: (a) 37% O_2/CO_2 (2ms, 6ms, 10ms, 14ms, 18ms), (b) 100% O_2 (3ms, 5ms, 7ms, 9ms, 11ms).

(a)

0.000   0.00750   0.0150   0.0225   0.0300

Particle releasing point and dropping direction

(b)

0.000   0.0075   0.015   0.022   0.0300

Figure 6. Spatio-temporal distribution of the mass fraction of H_2O: (a) 37% O_2/CO_2 (2ms, 6ms, 10ms, 14ms, 18ms), (b) 100% O_2 (3ms, 5ms, 7ms, 9ms, 11ms).

Figure 7. Spatio-temporal distribution of the mass fraction of H_2: (a) 37% O_2/CO_2 (2ms, 6ms, 10ms, 14ms, 18ms), (b) 100% O_2 (3ms, 5ms, 7ms, 9ms, 11ms).
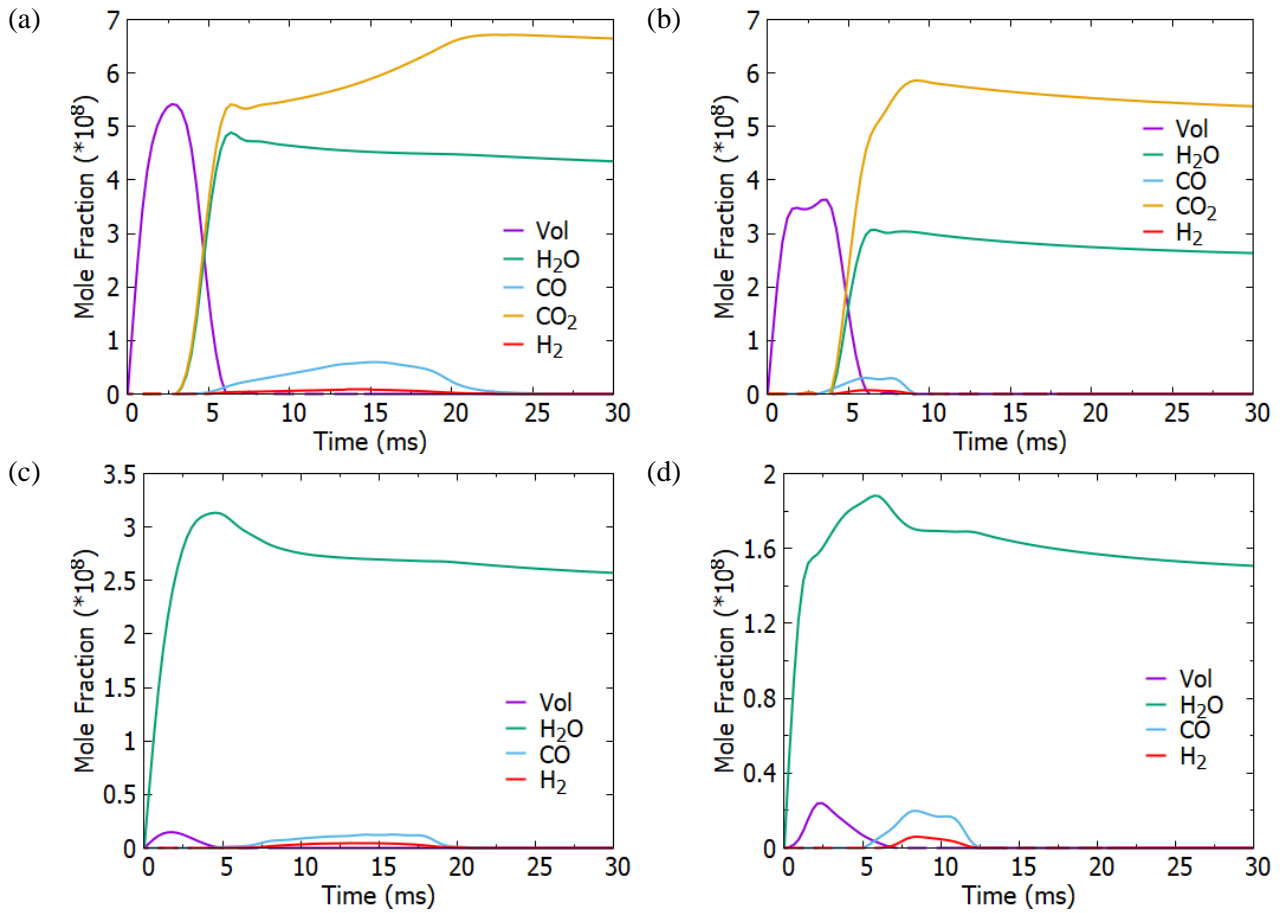
Figure 8. History of mass-averaged mole fraction of the major gaseous species during single biomass particle combustion: (a) 27% O_2 & 71% N_2, (b) 100% O_2, (c) 37% O_2 & 63% CO_2, (d) 77% O_2 & 23% CO_2.
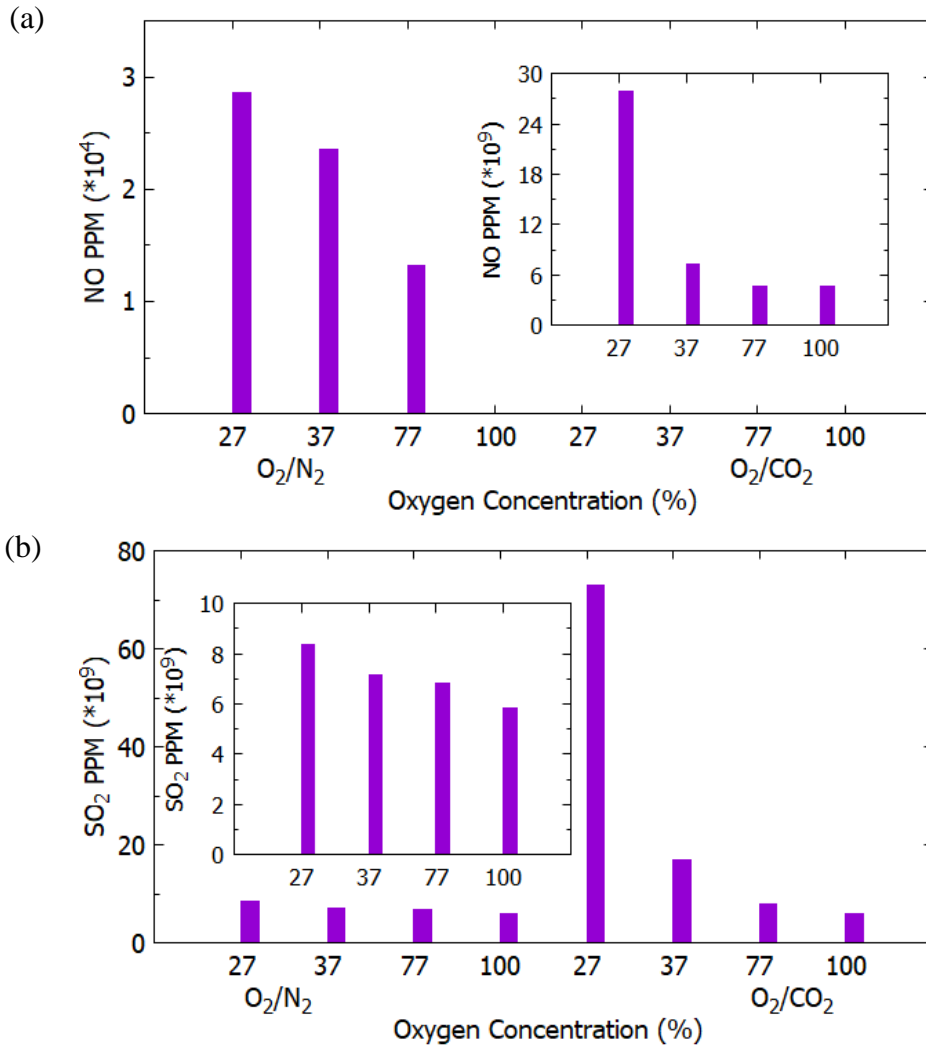
Figure 9. Overall PPM in different atmospheres during single Bagasse particle combustion. (a): NO, (b): SO_2.

(a)

(b)
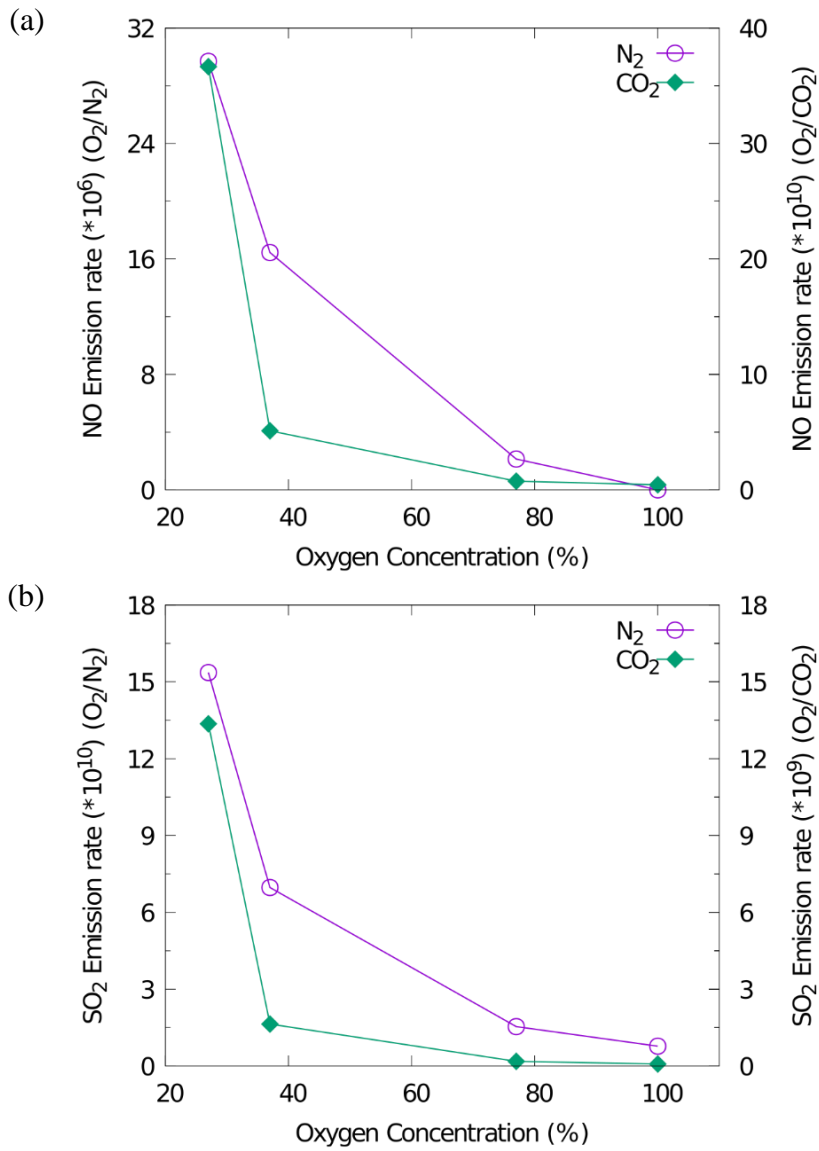
Figure 10. Species emission rates in different atmospheres during single Bagasse particle combustion. (a): NO, (b) SO_2.
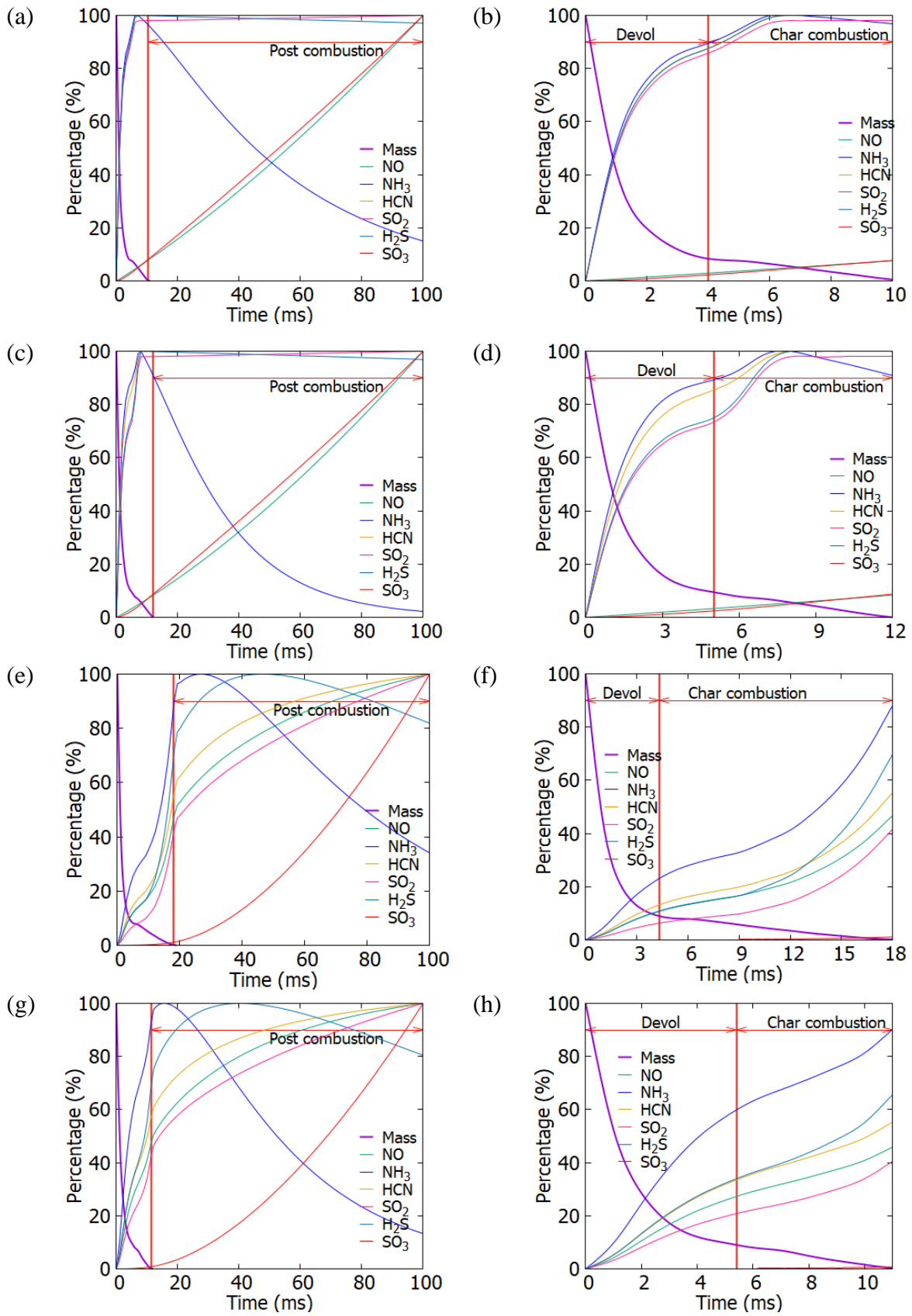
Figure 11. Species versus particle mass reduction during single Bagasse particle combustion. (a)-(b): 37% O_2 & 63% N_2, (c)-(d): 77% O_2 & 23% N_2, (e)-(f): 37% O_2 & 63% CO_2, (g)-(h): 77% O_2 & 23% CO_2.
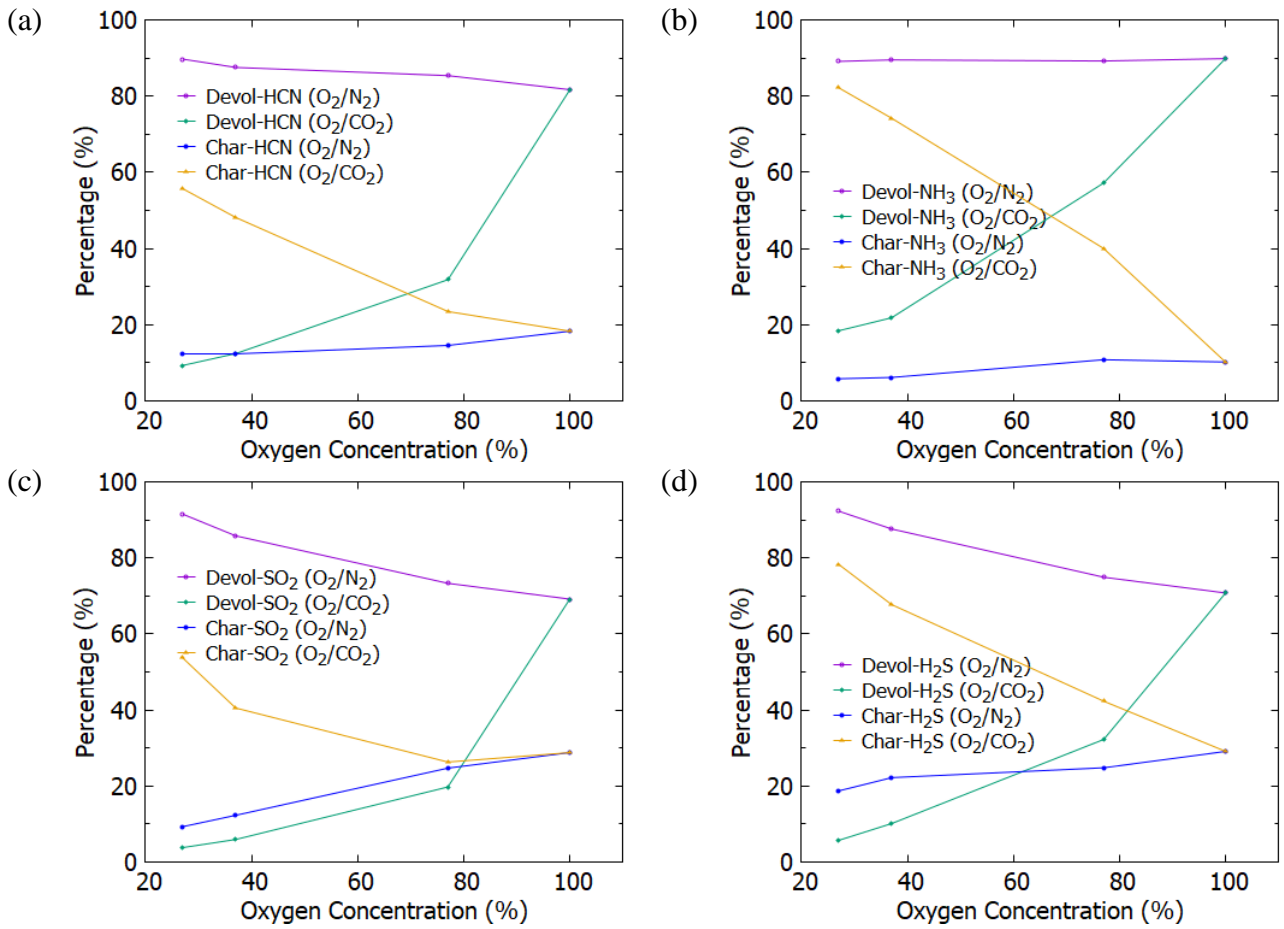
Figure 12. Species formation percentage for devolatilization and char combustion processes under different gas conditions. (a): HCN, (b): NH₃, (c): SO₂, (d): H₂S.

APPENDIX A: Validation of distribution assumption

As stated in Section 2.2 and 2.3, the nitrogen and sulphur contained in biomass particle are assumed to be distributed evenly between the volatile matters and the char. The mass fraction of nitrogen and sulphur in Bagasse particle, which was used in this work are given in Table 2, but the distributions of N and S in the volatiles and char are unknown. The specific distribution varies in different types of biomass fuel and it needs to be measured for each type. The total amounts of the NO_x and SO_x emissions are influenced by the distribution of N and S in the volatiles and char, and the partition fraction of intermediates. However, the trends under different fraction assumptions are nearly the same, as confirmed by Blaid[40] who ran five cases with different partition assumptions to match with the experimental results. In order to conduct the qualitative analysis of NO_x and SO_x emissions under various gas conditions, five kinds of partition assumptions of nitrogen and sulphur in the volatiles and char are used here to show that the changing trends of NO_x and SO_x emission are the same under different chemical composition of the surrounding atmospheres. The partition assumptions are shown in Table A1.

The changing trend of total mass fraction of NO and SO_2, and the percentage of NO and SO_2 formation during combustion under different gas conditions are used to validate the partition assumption. The compared results are shown in Figs. A1-A6. It is clear from these figures that, although the total amounts vary, the changing trends under varying gas conditions for different partition assumptions are the same. The results of HCN, NH_3, H_2S and SO_3 simulations support the same conclusion. For conciseness reasons, the equivalent figures are not shown here. This indicates that changes in distribution of nitrogen in the volatiles and char do not influence the qualitative analysis in any considerable way. Given this, a qualitative analysis to investigate the effects of oxygen concentration and CO_2 background gas on NO_x and SO_x emissions can be conducted based on a specified partition assumption.

Table A1. Partition assumptions of Nitrogen and Sulphur

	Case 1	Case 2	Case 3	Case 4	Case 5
Partition of Volatile-N	50%	30%	70%	50%	50%
Partition of Char-N	50%	70%	30%	50%	50%
Partition of HCN	50%	50%	50%	60%	30%
Partition of NH_3	10%	10%	10%	20%	30%
Partition of NO	40%	40%	40%	20%	40%
Partition of Volatile-S	33%	67%	50%	33%	33%
Partition of Char-S	67%	33%	50%	67%	67%
Partition of H_2S	40%	40%	40%	70%	50%
Partition of SO_2	60%	60%	60%	30%	50%
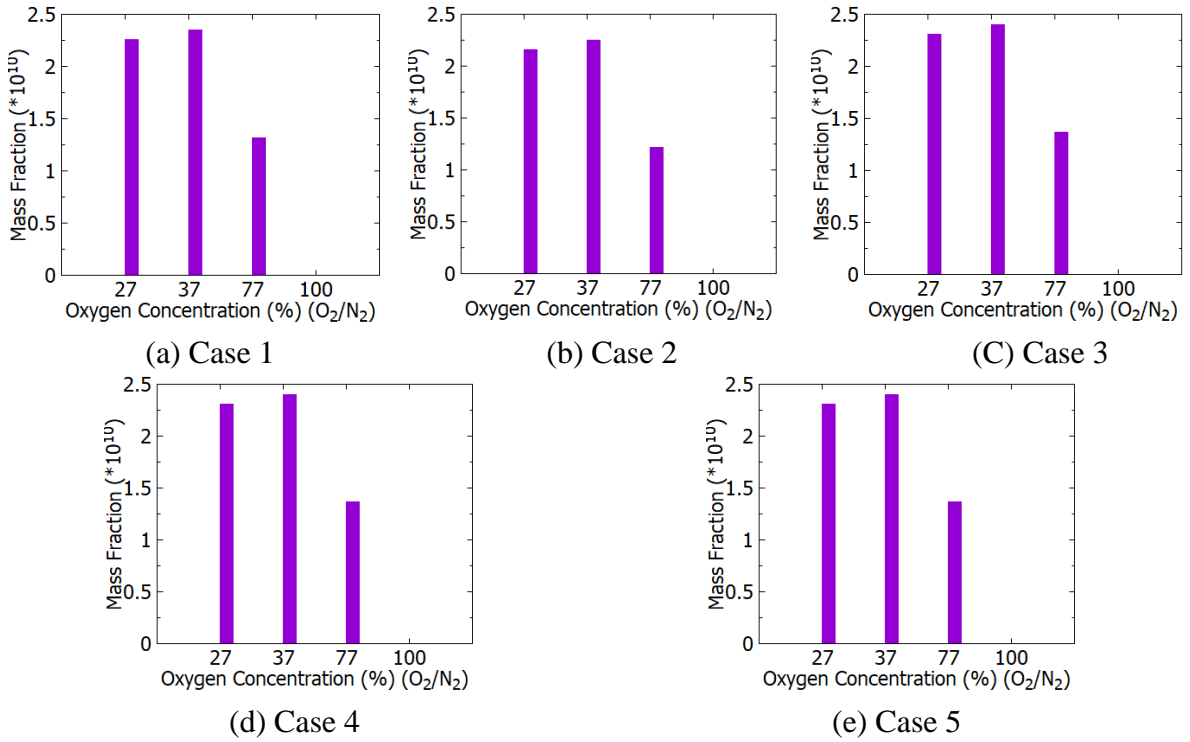
Figure A1. Mass fraction of NO in O_2/N_2 environments with partition assumptions (at t=100ms).
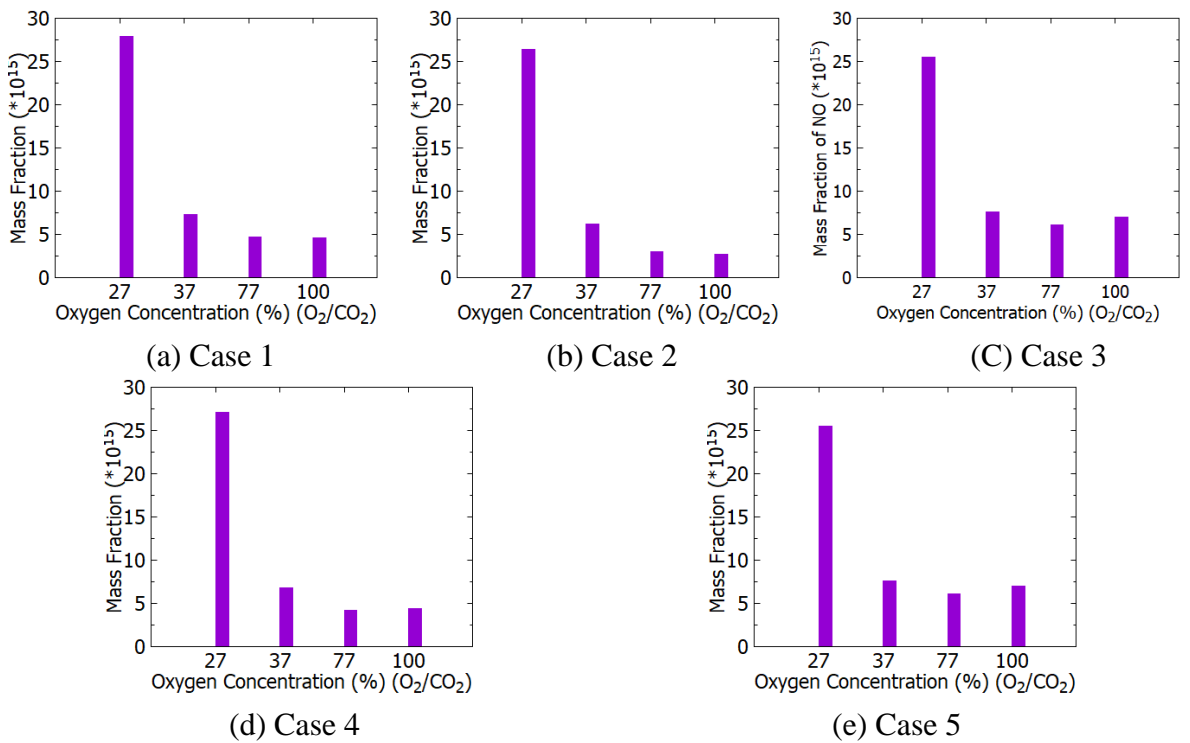
Figure A2. Mass fraction of NO in O_2/CO_2 environments with partition assumptions (at t=100ms).
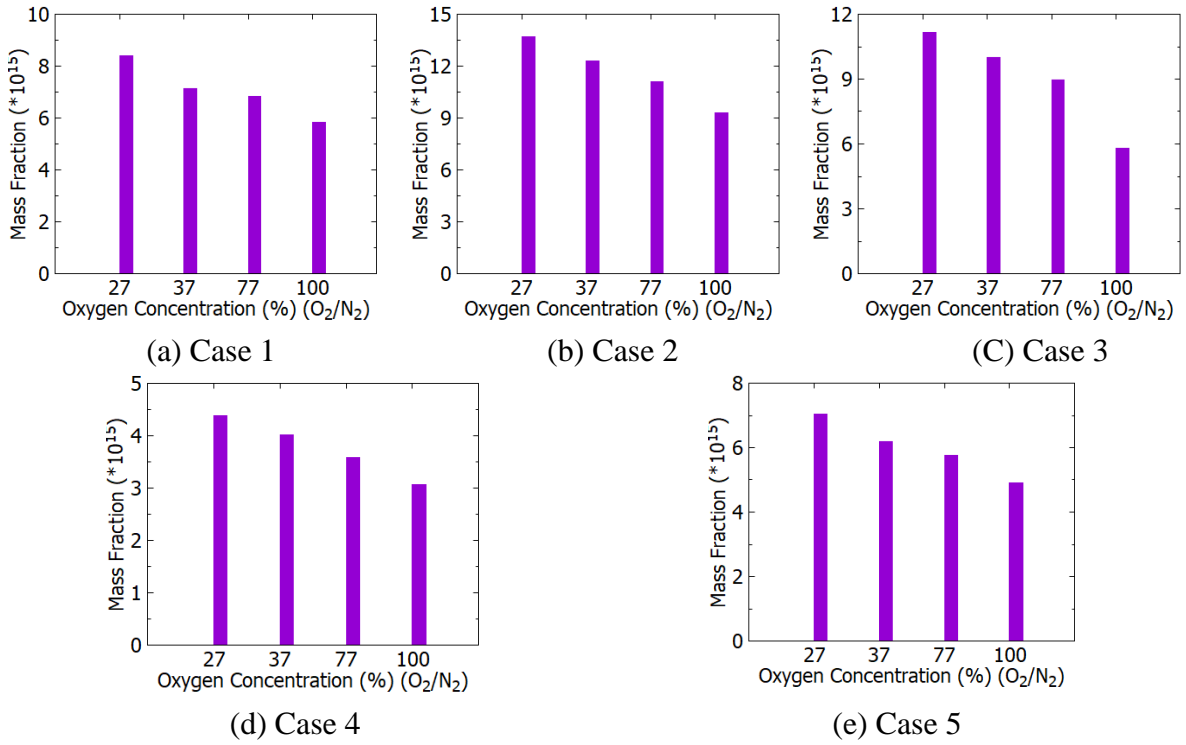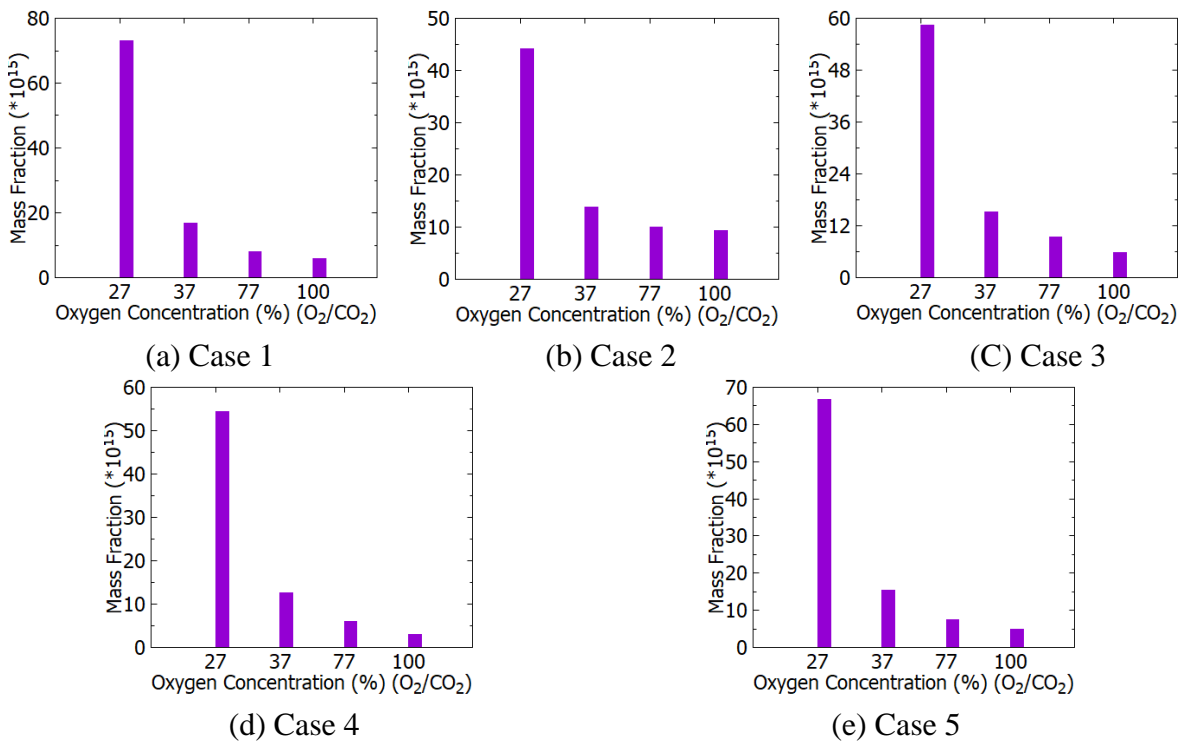
Figure A3. Mass fraction of SO_2 in O_2/N_2 environments with partition assumptions (at t=100ms).

Figure A4. Mass fraction of SO_2 in O_2/CO_2 environments with partition assumptions (at t=100ms).
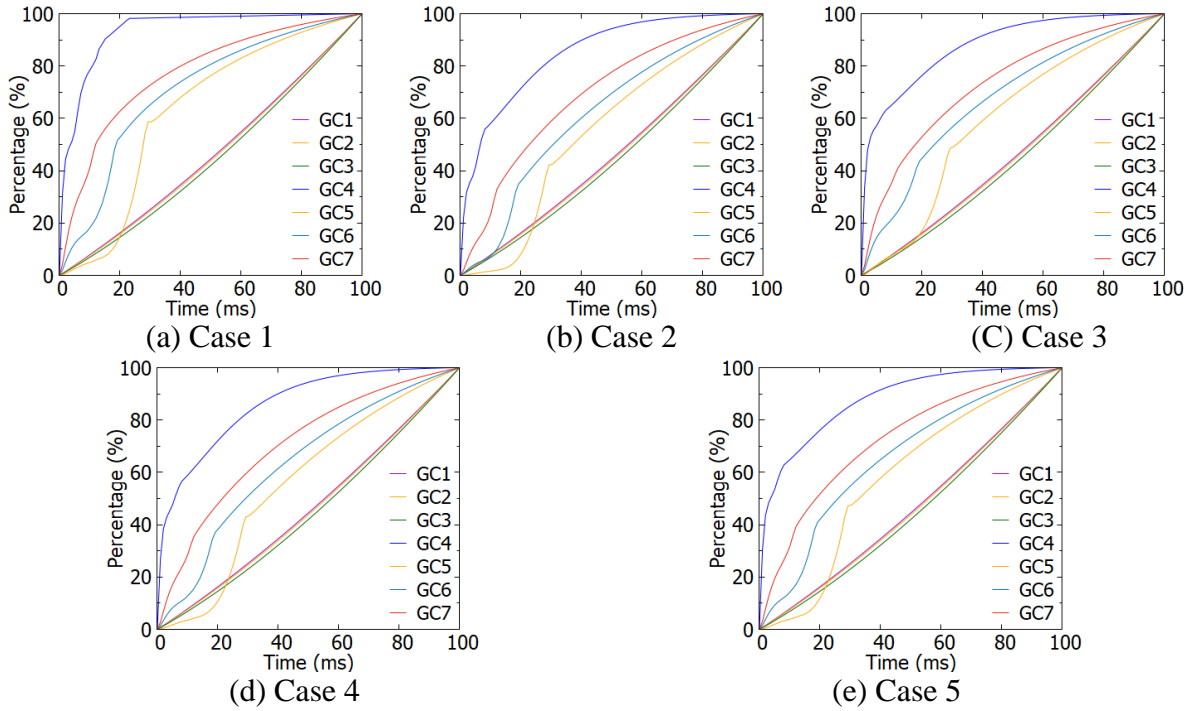
Figure A5. Percentage of NO formation during combustion process under varying gas conditions with partition assumptions. GC1: 27% O_2/N_2; GC2: 37% O_2/N_2; GC3: 77% O_2/N_2; GC4: 100% O_2; GC5: 27% O_2/CO_2; GC6: 37% O_2/CO_2; GC7: 77% O_2/CO_2.
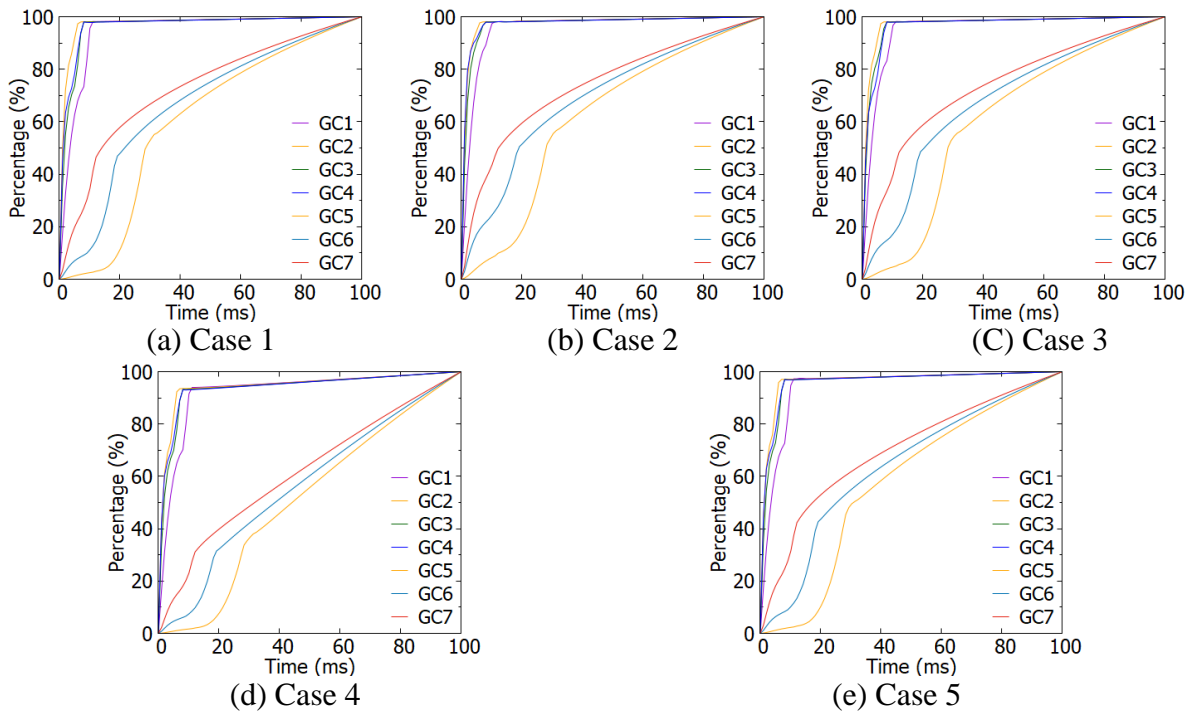

Figure A6. Percentage of SO_2 formation during combustion process under varying gas conditions with partition assumptions. GC1: 27% O_2/N_2; GC2: 37% O_2/N_2; GC3: 77% O_2/N_2; GC4: 100% O_2; GC5: 27% O_2/CO_2; GC6: 37% O_2/CO_2; GC7: 77% O_2/CO_2.